Mon. Not. R. Astron. Soc. **332,** 549–574 (2002)

Observations of the *Hubble Deep Field* South with the *Infrared Space Observatory* – II. Associations and star formation rates

Robert G. Mann,[1,2★] Seb Oliver,[1,3] Ruth Carballo,[4,5] Alberto Franceschini,[6] Michael Rowan-Robinson,[1] Alan F. Heavens,[2] Maria Kontizas,[7] David Elbaz,[8] Anastasios Dapergolas,[9] Evanghelos Kontizas,[9] Gian Luigi Granato,[6] Laura Silva,[10] Dimitra Rigopoulou,[11] J. Ignacio Gonzalez-Serrano,[5] Aprajita Verma,[1,11] Steve Serjeant,[1,12] Andreas Efstathiou[1] and Paul P. van der Werf[13]

[1]*Astrophysics Group, Imperial College London, Blackett Laboratory, Prince Consort Road, London SW7 2BZ*
[2]*Institute for Astronomy, University of Edinburgh, Royal Observatory, Blackford Hill, Edinburgh EH9 3HJ*
[3]*Astronomy Centre, School of Chemistry, Physics and Environmental Science, University of Sussex, Falmer, Brighton BN1 9QJ*
[4]*Departamento de Matematica Aplicada y CC, Universidad de Cantabria, Avda. Los Castros s/n, 39005 Santander, Spain*
[5]*Instituto de Física de Cantabria (CSIC-UC), Avda. Los Castros s/n, 39005 Santander, Spain*
[6]*Dipartimento di Astronomia, Universita' di Padova, Vicolo dell'Osservatorio 5, I-35122, Padova, Italy*
[7]*Department of Physics, University of Athens, Panepistimiopolis, GR-15783, Zografos, Greece*
[8]*DSM/DAPNIA/SAp, CE–Saclay, Orme des Merisiers – Bat 709, 91191 Gif-sur-Yvette Cedex, France*
[9]*Astronomical Institute, National Observatory of Athens, Lofos Nymfon, Thission, PO Box 20048, 11810 Athens, Greece*
[10]*Astrophysics Sector, SISSA, Via Beirut 2-4, 34013 Trieste, Italy*
[11]*Max-Planck-Institut für extraterrestrische Physik, Postfach 1603, 85740 Garching, Germany*
[12]*Unit for Space Sciences and Astrophysics, School of Physical Sciences, University of Kent, Canterbury CT2 7NZ*
[13]*Leiden Observatory, PO Box 9513, NL-2300 RA Leiden, the Netherlands*

Accepted 2001 December 19. Received 2001 December 19; in original form 2001 June 19

ABSTRACT

We present results from a deep mid-infrared survey of the *Hubble Deep Field* South (HDF-S) region performed at 6.7 and 15 μm with the ISOCAM instrument on board the *Infrared Space Observatory* (*ISO*). We find reliable optical/near-infrared associations for 32 of the 35 sources detected in this field by Oliver et al. (Paper I): eight of them are identified as stars, one is definitely an active galactic nucleus (AGN), a second seems likely to be an AGN too, while the remaining 22 appear to be normal spiral or starburst galaxies. Using model spectral energy distributions (SEDs) of similar galaxies, we compare methods for estimating the star formation rates (SFRs) in these objects, finding that an estimator based on integrated (3–1000 μm) infrared luminosity reproduces the model SFRs best. Applying this estimator to model fits to the SEDs of our 22 spiral and starburst galaxies, we find that they are forming stars at rates of $\sim 1-100\,\mathrm{M_\odot\,yr^{-1}}$, with a median value of $\sim 40\,\mathrm{M_\odot\,yr^{-1}}$, assuming an Einstein–de Sitter universe with a Hubble constant of $50\,\mathrm{km\,s^{-1}\,Mpc^{-1}}$, and star formation taking place according to a Salpeter initial mass function (IMF) across the mass range $0.1-100\,\mathrm{M_\odot}$. We split the redshift range $0.0 \leq z \leq 0.6$ into two equal-volume bins to compute raw estimates of the star formation rate density, $\dot{\rho}_*$, contributed by these sources, assuming the same cosmology and IMF as above and computing errors based on estimated uncertainties in the SFRs of individual galaxies. We compare these results with other estimates of $\dot{\rho}_*$ made with the same assumptions, showing them to be consistent with the results of Flores et al. from their *ISO* survey of the CFRS 1415+52 field. However, the relatively small volume of our survey means that our $\dot{\rho}_*$ estimates suffer from a large sampling variance, implying that our results, by themselves, do not place tight constraints on the global mean star formation rate density.

★E-mail: rgm@roe.ac.uk

Key words: surveys – galaxies: evolution – galaxies: formation – galaxies: Seyfert – galaxies: starburst – infrared: galaxies.

1 INTRODUCTION

In an accompanying paper (Oliver et al. 2002, hereafter Paper I) we described the survey we made of the *Hubble Deep Field* South (HDF-S) region[1] using the LW2 (centred at 6.7 μm) and LW3 (15 μm) filters of the ISOCAM (Cesarsky et al. 1996) instrument on board the *Infrared Space Observatory* (*ISO*) (Kessler et al. 1996). A prime motivation for this project came from the results of previous *ISO* surveys, such as our own survey (Serjeant et al. 1997; Goldschmidt et al. 1997; Oliver et al. 1997; Mann et al. 1997; Rowan-Robinson et al. 1997) of the northern *Hubble Deep Field* (HDF-N, Williams et al. 1996) and that of Flores et al. (1999) in the Canada–France Redshift Survey 1415+52 field (Lilly et al. 1995), which revealed an infrared luminosity density at $0.5 \lesssim z \lesssim 1$ implying a higher star formation rate (SFR) density at those redshifts than indicated by previous optical studies (e.g. Lilly et al. 1996; Madau et al. 1996; Connolly et al. 1997).

These studies were facilitated by the availability of multi-wavelength data sets in those well-studied fields, which made possible the association of *ISO* sources with galaxies for which redshifts had been determined through optical spectroscopy or for which they could be estimated on the basis of multiband optical/near-infrared photometry. The same factors favour the study of the HDF-S region, and in this paper we discuss the association of our *ISO* sources in the HDF-S with objects in optical and near-infrared catalogues of that field, and the estimation of their SFRs. This process is significantly easier than was the case for our survey of the northern HDF-N, since, as emphasized in Paper I, our *ISO* data set in the HDF-S is greatly superior, as a result of an observational strategy and data reduction procedure both revised significantly in the light of developing knowledge of the characteristics of the ISOCAM instrument and of the source population that it probed.

The plan of the rest of this paper is as follows. In Section 2, we describe the existing optical and near-infrared catalogues in the HDF-S region with which we shall seek associations for our *ISO* sources, review the likelihood ratio method used to obtain them and present the results of its application. In Section 3 we compare a variety of commonly used SFR estimators, through applying them to model spectral energy distributions (SEDs), while in Section 4 we apply the best of them to the multi-wavelength photometric data sets compiled for the galaxies with which we have associated our *ISO* sources, to yield estimates of their SFRs, and in Section 5 we use these results to assess the contribution of *ISO*-selected sources to the star formation history of the HDF-S. Finally, in Section 6, we discuss the results of this paper and the conclusions that we draw from them. Appendices present mathematical details of the processes of correcting an SFR estimate to a canonical initial mass function (IMF), and of computing the sampling variance in estimates of the SFR density using a lognormal model for the cosmological density field.

[1] See www.stsci.edu/ftp/science/hdfsouth/hdfs.html

2 OPTICAL CATALOGUES AND ASSOCIATIONS

As shown in Fig. 1, the region within which the final source catalogue of Paper I was selected is covered by a number of optical and near-infrared imaging surveys, and we have sought to associate our *ISO sources* with *objects* detected in all of them, using the likelihood ratio method detailed by Sutherland & Saunders (1992).

2.1 Method

The implementation of the likelihood ratio association technique used here is essentially identical to that we used for the *ISO* HDF-N sources in Mann et al. (1997), so we only briefly review it here. The likelihood ratio, *LR*, for the association of a particular source with a given catalogue object is defined to be the ratio, $p_{\rm true}/p_{\rm chance}$, of the infinitesimal probability of finding the true counterpart to the source at the position of the object and with its flux to the infinitesimal probability of an object with that flux being found there by chance. Sutherland & Saunders (1992) showed that it

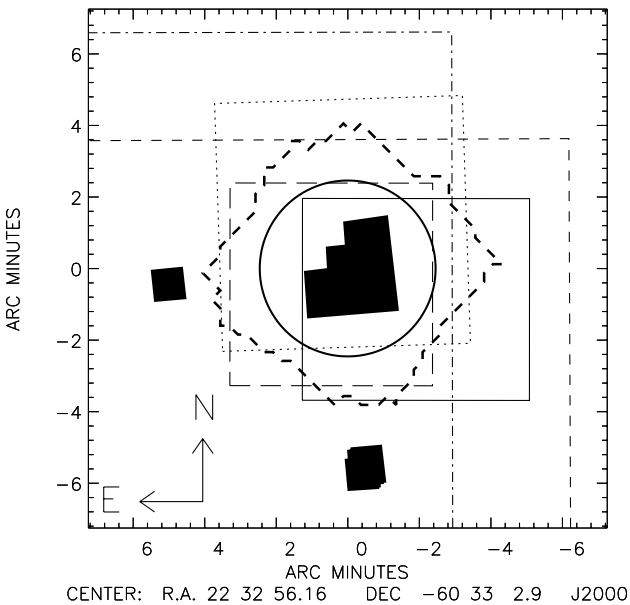

Figure 1. The location of our *ISO* rasters with respect to those of other data sets taken in the area. The shaded regions mark the *HST* fields, with the STIS and NICMOS fields to the east and south of the WFPC2 field, respectively. The thick-dashed irregular shape and the solid circle show, respectively, the maximum extent of our *ISO* coverage (the coverage in the two bands differs slightly) and the region from which the source catalogues of Paper I were selected. The remaining lines show boundaries of four optical/near-infrared surveys discussed in Section 2, as follows: (i) dotted line – AAT prime focus imaging survey of Verma et al. (in preparation); (ii) dashed line – CTIO BTC survey of Gardner et al. (1999); (iii) dot–dashed line – CTIO BTC survey of Walker (1999); (iv) solid line – ESO EIS optical imaging survey of da Costa et al. (1998); and (v) long-dashed line – ESO EIS near-infrared survey of da Costa et al. (1998).

takes the form

$$LR(f,x,y) = \frac{q(f)e(x,y)}{n(f)}, \quad (1)$$

where $e(x,y)$ is the probability distribution for positional offsets, (x,y), between source and object [normalized so that $\int e(x,y)\,\mathrm{d}x\,\mathrm{d}y = 1$ with the integral being taken over all space], $n(f)$ is the surface density of objects per unit interval in flux, f, and $q(f)$ is the probability distribution function for an ensemble of sources, measured in the same passband in which the object catalogue is defined.

The quantity $q(f)$ essentially measures the flux distribution of the true counterparts of the sources in the object catalogue, and is unknown unless associations have previously been found between an ensemble of similar sources and a catalogue of similar objects. Sutherland & Saunders (1992) suggested that it may be estimated in binned form by subtracting from the flux histogram of the objects lying near the source positions that for the full object catalogue. If the latter is scaled to cover the same area as used to compute the former, then the resulting quantity is proportional to $q(f)$, exhibiting an excess of galaxies in the bins corresponding to the fluxes of the true counterparts of the sources in the object catalogues. Mann et al. (1997) showed that, when applied to relatively small source samples, such as in our *ISO* surveys of the two HDFs, this empirical $q(f)$ is very noisy, and they preferred to take $q(f)$ to be a constant, independent of flux. Since their fig. 1 strongly implied that the *ISO* HDF-N sources were associated with objects brighter than $I_{814} \simeq 23$ in the catalogue of Williams et al. (1996), this assumption would have led them to underestimate the value of $p_{\rm true}$ for bright objects, but, in practice, this was seen to have no effect on the associations made, so we follow the same procedure here. The validity of making that same simplifying assumption here is illustrated by Fig. 2, where we compare the R-band magnitude distribution near (defined to be within 6 arcsec of) the 30 *ISO* sources from table 8 of Paper I contained within the area of the Gardner et al. (1999) catalogue, and that for the catalogue as a whole. This shows the strong excess of bright ($R = 19$–21) objects near *ISO* source positions – a two-sided Kolmogorov–Smirnov test gives a probability of $P \sim 10^{-10}$ that these two are drawn from the same parent distribution – which gives us confidence both in the reliability of our source detections and in our adoption of a constant $q(f)$ here.

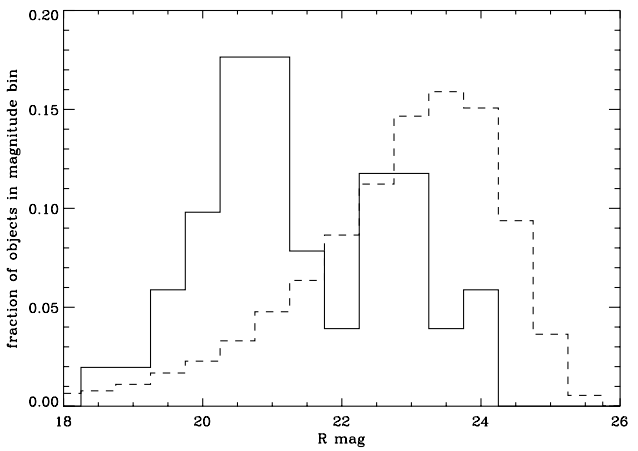

Figure 2. A comparison of (solid line) the R-band magnitude distribution of the objects within circles of radius 6 arcsec around the 30 *ISO* sources from table 8 of Paper I contained within the area of the Gardner et al. (1999) catalogue, and (dashed line) that for the catalogue as a whole, showing the strong excess of bright objects near *ISO* source positions: a two-sided Kolmogorov–Smirnov test gives a probability of $P \sim 10^{-10}$ that these two are drawn from the same parent distribution.

For each association made between a given *ISO* HDF-N source and a particular object in the I_{814}-band catalogue of Williams et al. (1996), Mann et al. (1997) computed the probability, $P_{\rm ran}(I_{814})$, that a fictitious source, placed at random in the HDF-N, would have a likeliest association with an object in the I_{814}-band catalogue producing a likelihood ratio at least as high as that for the source and object in question. Clearly, $P_{\rm ran}$ combines information as to the reliability of the source detection as well as the probability that the given object is the correct counterpart of the source, but, as discussed below, it provides a useful measure of the quality of the associations made in this case; a more direct measure would be available (Sutherland & Saunders 1992; Rutledge et al. 2000) if we could compute our *LR* values using a good estimate of $q(f)$, but, as mentioned above, the small number of sources here leads us to take $q(f)$ to be a constant, thereby leaving *LR* defined only up to a multiplicative factor, in which case we cannot employ the formalism of Sutherland & Saunders (1992) or Rutledge et al. (2000) for quantifying the reliability of associations.

We sought associations for our *ISO* sources with objects in the following set of catalogues: (i) the R-band Anglo-Australian Telescope (AAT) prime-focus catalogue of Verma et al. (in preparation); (ii) the I_{814}-band STScI *HST* catalogue:[2] (iii) the I-band ESO Imaging Survey (EIS) catalogue of da Costa et al. (1998); (iv) the K-band EIS catalogue of da Costa et al. (1998); and (v) the R-band CTIO Big Throughput Camera (BTC) catalogue (version 2) of Gardner et al. (1999).[3] Inspection of the results of this process revealed that almost all of the *ISO* sources were associated with the same star or galaxy in each case, indicating the robustness of this method of association. Moreover, the associations made using the different catalogues in their different bands yielded very similar $P_{\rm ran}$ values for the associations between given pairs of source and object, giving us confidence that it is a sound statistic to use.

2.2 Results

As mentioned above, very similar $P_{\rm ran}$ results are obtained for our sources when the likelihood ratio procedure is run against all five optical and near-infrared catalogues listed in the previous subsection. We take our principal association to be with the R-band CTIO BTC catalogue of Gardner et al. (1999), simply because it includes the largest number of the objects associated with our sources. In Fig. 3 we plot the histogram of $P_{\rm ran}$ values resulting from the association of the *ISO* sources in table 8 of Paper I with objects in the CTIO catalogue. A few of our sources are clearly associated with objects in regions of the image masked out by Gardner et al. (1999) when they constructed their SExtractor (Bertin & Arnouts 1996) catalogue from it: for these cases we use the $P_{\rm ran}$ value for associated EIS K- or I-band object instead. This histogram is similar to what we should expect: most of the *ISO* sources have been associated with objects with low $P_{\rm ran}$ values, indicating a high probability that this is a correct identification, while there is a tail to high $P_{\rm ran}$, owing to sources that either are spurious or have optical counterparts too faint for detection in the CTIO image, which has a limiting magnitude of $R \sim 23$. The $P_{\rm ran}$

[2] Available from the STScI HDF-S web site at http://www.stsci.edu/ftp/science/hdfsouth/catalogs.html

[3] Available from http://hires.gsfc.nasa.gov/~research/hdfs-btc/

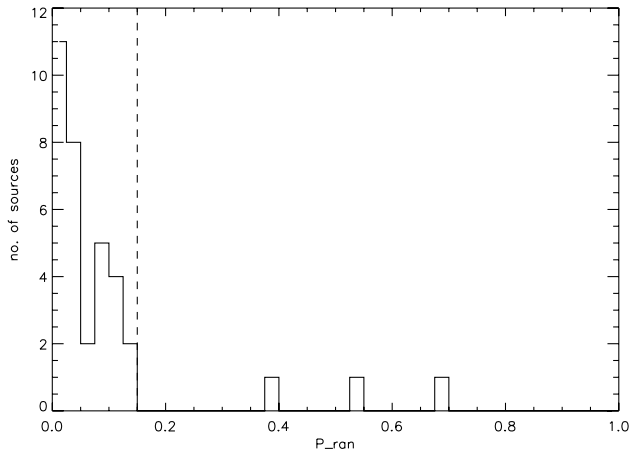

Figure 3. The $P_{\rm ran}$ histogram for the associations made between the 35 sources in table 8 of Paper I and the *R*-band catalogue of Gardner et al. (1999), supplemented by the ESO EIS *K*- or *I*-band catalogue for those sources falling into the masked region of the Gardner et al. image. We define good associations to be those with $P_{\rm ran} < 0.15$, to the left of the dashed line.

value to be taken as the threshold below which associations are defined to be good is somewhat arbitrary when the number of sources is low, as here; with a much larger number it is possible to see the point where the number of sources begins significantly to exceed the flat tail resulting from sources that are spurious or have no counterpart in the object catalogue, but that is clearly not possible in Fig. 3. The form of that histogram suggests that $P_{\rm ran} = 0.15$ might be an appropriate threshold. Note that Mann et al. (1997) took their threshold for reasonable identifications of *ISO* HDF-N sources to be 0.35, so the much tighter bunching to lower $P_{\rm ran}$ values here indicates once more that the *ISO* data presented here are of a far higher quality than those used in the initial *ISO* HDF-N analysis. In particular we have benefited from the knowledge of the ISOCAM image distortion which was uncharacterized at the time that Mann et al. (1997) performed their identification of the optical counterparts of the *ISO* HDF-N sources.

In Fig. 4 we show postage stamp images for the 32 sources in Paper I with reliable associations, overlaying *ISO* 6.7- and 15-μm contours on to optical images, with the associated object lying at (0, 0). Table 1 summarizes the properties of these objects, while the next subsection presents more details of the associations. As mentioned previously, principal associations were made with the Goddard Space Flight Centre (GSFC) *R*-band catalogue of Gardner et al. (1999), so the optical magnitudes tabulated are from their catalogue, with one exception (ISOHDFS J223237-603235), which is omitted from their catalogue, causing us to use the EIS optical catalogue of da Costa et al. (1998). The photometric data in the GSFC catalogue are calibrated using standards measured in Johnson *UBV* and Cousins *RI*, so we quote all optical magnitudes in that system. For the one case of ISOHDFS J223237-603235, this involves converting the *UBVRI* magnitudes back to the Johnson–Cousins system from the AB system in which da Costa et al. (1998) present their photometry, using the conversions given in their paper, namely $U = U_{\rm AB} - 0.82$, $B = B_{\rm AB} + 0.06$, $V = V_{\rm AB}$, $R = R_{\rm AB} - 0.17$ and $I = I_{\rm AB} - 0.42$. For their near-infrared data, da Costa et al. (1998) performed photometric calibration in *JHK* using Persson et al. (1998) standards and then converted them to AB magnitudes; again we have reversed this conversion, using the relations quoted by da Costa et al. (1998), namely $J = J_{\rm AB} - 0.89$, $H = H_{\rm AB} - 1.38$ and $K = K_{\rm AB} - 1.86$. In Table 1 we present spectroscopic redshifts from Glazebrook et al. (in preparation) where available, and photometric redshifts where not. Photometric redshifts were estimated by three of us, using independent methods: M. Rowan-Robinson (MRR) used (Rowan-Robinson 2001) SEDs based on those of Yoshii & Takahara (1988), A. Franceschini (AF) used the PEGASE models of Fioc & Rocca-Volmerange (1997), and R. G. Mann (RGM) used the GRASIL (Silva et al. 1998) model fits to SEDs of a range of known galaxies (Arp 220, M100, M51, M82, NGC 6090, NGC 6946) presented by Silva et al. (1998). Results for individual galaxies are discussed below, but, in most cases, these independent methods yielded photometric redshift estimates that agreed with each other, and with those computed by Stephen Gwyn (Gwyn 1999) and the State University of New York (SUNY) group,[4] to $\delta z \sim 0.1$, which is therefore the accuracy that we claim for the adopted photometric redshifts listed in parentheses in Table 1.

2.3 Notes on individual sources

(i) *ISOHDFS J223237-603235.* The association here is with an $I = 16$ star, 2 arcsec from the *ISO* source position and yielding $P_{\rm ran} = 0.001$ from the EIS optical catalogue (the star is masked out of the CTIO catalogue).

(ii) *ISOHDFS J223237-603256.* As shown by the contours in Fig. 4, this 6.7-μm source is very safely ($P_{\rm ran} = 0.001$) associated with a bright (17th magnitude in *R*) object clearly identified as a star by SExtractor in the AAT *R* and EIS *I* images.

(iii) *ISOHDFS J223240-603141.* This 15-μm source is associated fairly securely ($P_{\rm ran} = 0.095$) with an $I = 20$ galaxy, located 3 arcsec from the *ISO* position. MRR estimates $z_{\rm phot} = 2.02$ for this galaxy, on the basis of its *UBVRI* magnitudes, while both AF and RGM estimate 0.45, so it is this latter figure that we adopt: as shown in Fig. 6 (later), with this assumed redshift, the optical and *ISO* data for this galaxy are well fitted by the GRASIL model for NGC 6090.

(iv) *ISOHDFS J223243-603242.* This is an $I = 20$ galaxy, detected significantly ($>4\sigma$) in the co-added maps at both 6.7 and 15 μm. This association yields $P_{\rm ran} = 0.047$, and MRR and AF both estimate a photometric redshift of $z_{\rm phot} = 0.5$ from the optical/near-infrared data for this galaxy, while RGM obtains a slightly lower value of 0.45: we adopt 0.5, and show in Fig. 6 (later) that, with this redshift, the *U*-band to 6.7-μm data are in good agreement with the GRASIL model for the starburst galaxies (Arp 220, M82, NGC 6090).

(v) *ISOHDFS J223243-603351.* Another very significant detection at both 6.7 and 15 μm, this source is associated ($P_{\rm ran} = 0.028$) with a 19th-magnitude galaxy, with detections at both 4.9 and 8.6 GHz (with fluxes of 0.163 and 0.111 mJy respectively: A. Hopkins, private communication). Its spectrum exhibits one broad line, and yields a redshift of $z = 0.0918$, so this appears to be a low-redshift AGN: RGM, AF and MRR estimate $z_{\rm phot} = 0.00, 0.15$ and 0.12, respectively.

(vi) *ISOHDFS J223243-603441.* This source, detected very significantly in both *ISO* bands, is associated ($P_{\rm ran} = 0.021$) with the brighter (19th magnitude in *I*) of a close pair of galaxies, for which RGM, AF and MRR estimate $z_{\rm phot} = 0.40, 0.50$ and 0.59, respectively, on the basis of *UBVRIJHK* photometry. We adopt $z = 0.5$ and show in Fig. 6 (later) that this gives this galaxy an SED more like the cirrus galaxy M51 than the starbursts.

[4] See www.ess.sunysb.edu/astro/hdfs/home.html

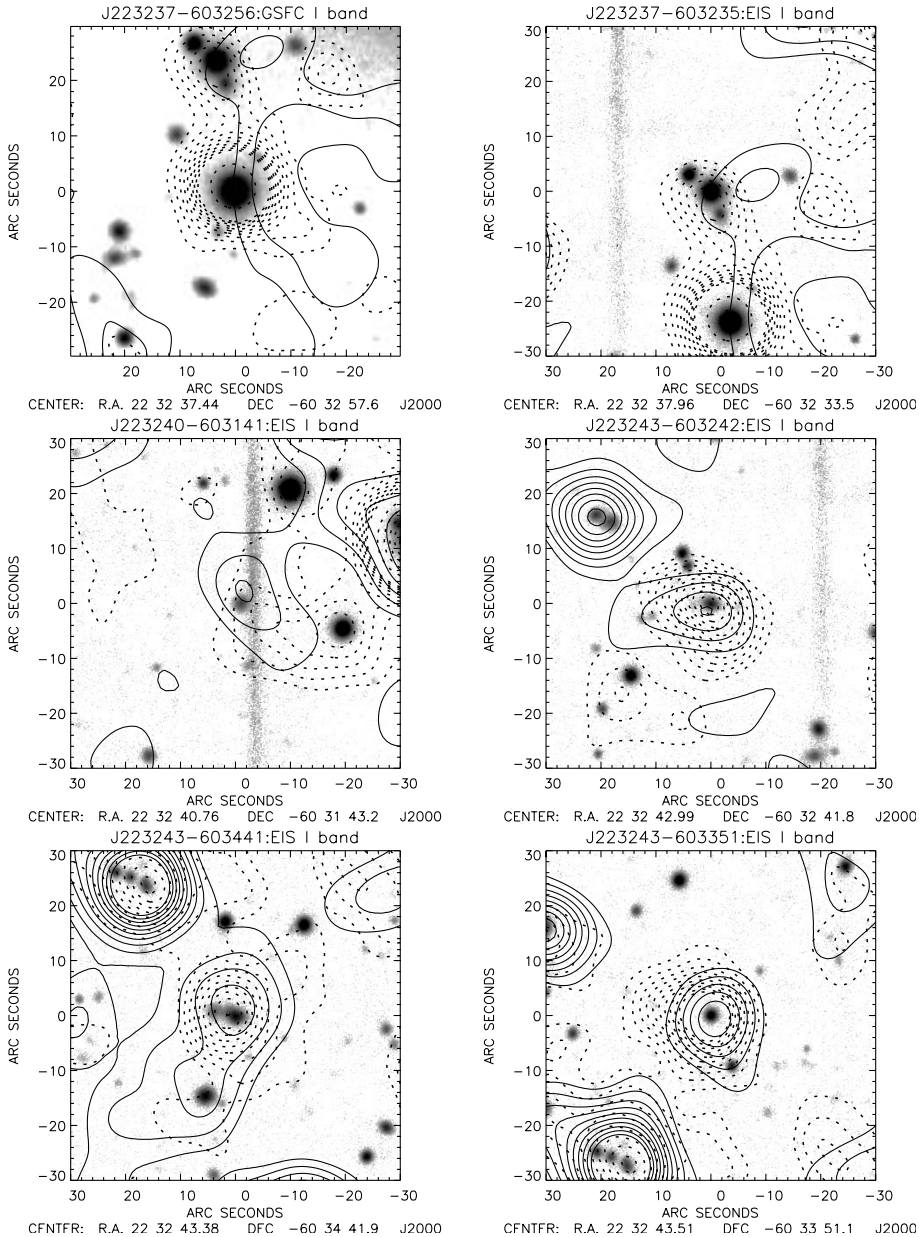

Figure 4. Postage stamp images for the 32 sources from Paper I with reliable associations. *ISO* contours (1, 2, 3, . . ., 9, 10, 20, . . ., 90, 100, 200) from the 6.7-μm (dashed) and 15-μm (solid) signal-to-noise ratio map are plotted over an optical/near-infrared image, centred on the object associated with the *ISO* source; the title of each image gives the name of the *ISO* source and the optical/near-infrared image used for the background.

(vii) *ISOHDFS J223244-603110.* This source, solidly detected at 15 μm, is located 3 arcsec from an $I = 20$ galaxy, with which we associate it securely ($P_{\rm ran} = 0.066$). The *UBVRIJHK* photometry for this galaxy yields a fairly wide spread of photometric redshift estimates, with RGM, AF and MRR obtaining 0.10, 0.25 and 0.32, respectively. We adopt the middle value, using which the SED of the galaxy is seen to be similar to that of the GRASIL fit to the starburst NGC 6090, and note that this is one of our more uncertain redshift estimates.

(viii) *ISOHDFS J223244-603455.* This 15-μm source is associated with an $I = 19$ galaxy 2 arcsec from the *ISO* position, with a $P_{\rm ran}$ value of 0.031, and *UBVRIJHK* magnitudes yielding photometric redshift estimates of 0.32, 0.30 and 0.45 from MRR, RGM and AF, respectively. A value of $z_{\rm phot} = 0.35$ is adopted, with which the SED of this galaxy matches that of the GRASIL model for the normal spiral M100, as shown in Fig. 6 (later).

(ix) *ISOHDFS J223245-603226.* This 15-μm source is associated with one of a pair of close (interacting?) galaxies, with $I = 20$ and $P_{\rm ran} = 0.080$, for which RGM, AF and MRR estimate photometric redshifts of 0.50, 0.50 and 0.51. Rigopoulou et al. (2001) measured a spectroscopic redshift of $z = 0.59$, and, using that value, the SED of this galaxy is a reasonable fit to the GRASIL model SED for the starburst NGC 6090.

(x) *ISOHDFS J223245-603418.* This is an $I = 20$ galaxy, detected at both 6.7 and 15 μm, yielding $P_{\rm ran} = 0.076$, with a spectrum showing Hβ and O III (4959+5007) lines, from which a redshift of $z = 0.4606$ was determined: RGM, AF and MRR estimate $z_{\rm phot} = 0.55, 0.6$ and 0.95, respectively, for this source.

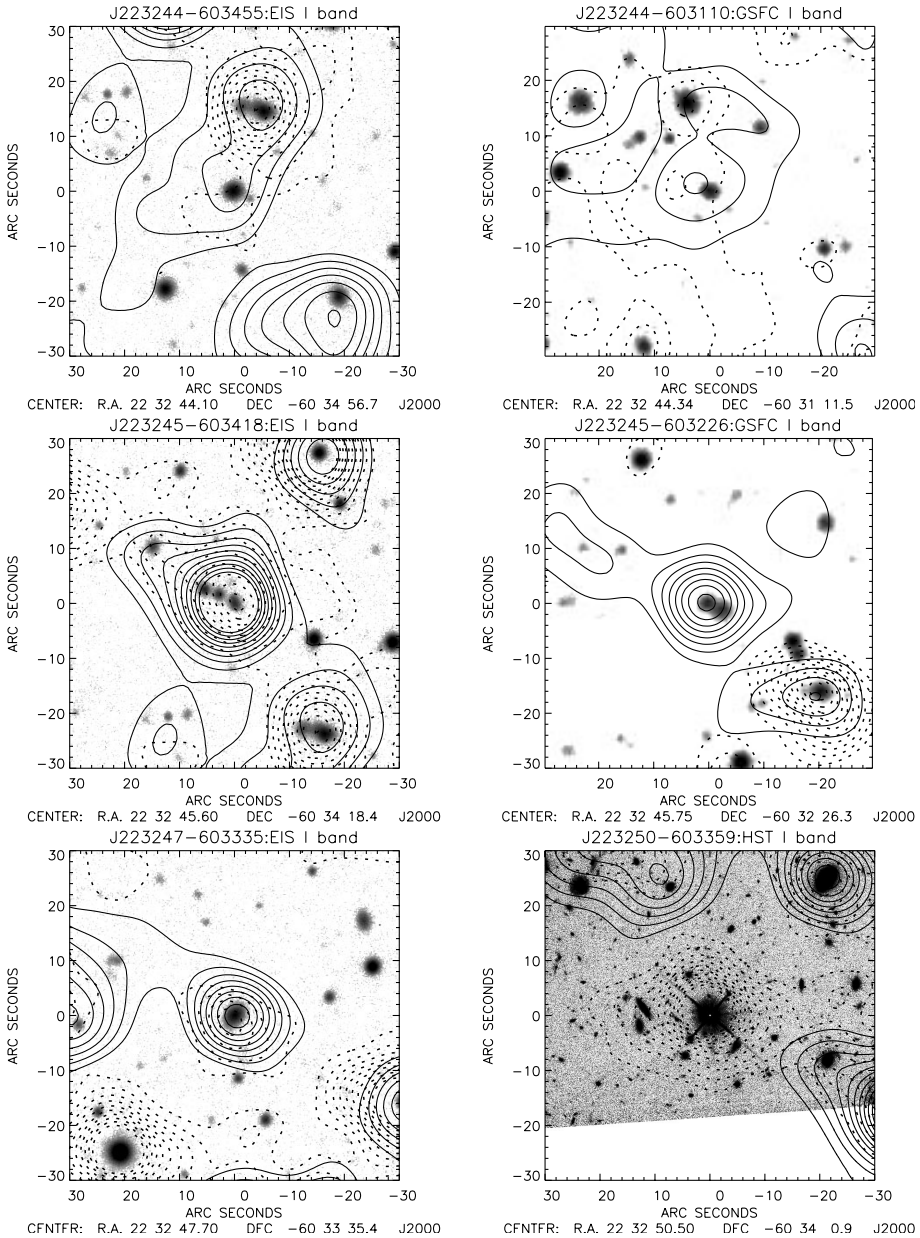

Figure 4 – *continued*

This is also a radio source, detected at 1.4, 2.5 and 4.9 GHz, with fluxes of 0.200, 0.149 and 0.127 mJy, respectively (A. Hopkins, private communication). As shown by Fig. 6 (later), the SED of this galaxy is in good agreement with the GRASIL model for Arp 220 over six decades in wavelength.

(xi) *ISOHDFS J223247-603335.* Detected at both 6.7 and 15 μm, we associate ($P_{\rm ran} = 0.029$) this source with an $I = 19$ galaxy, with a spectrum displaying a number of emission lines and yielding a redshift of $z = 0.5803$: RGM AF, MRR, Gwyn (1999) and the SUNY group estimated photometric redshifts of 0.50, 0.60, 0.52, 0.56 and 0.66, respectively, for this galaxy, the SED of which is similar to that of the GRASIL model for the spiral galaxy M51.

(xii) *ISOHDFS J223250-603359.* This 6.7-μm source is associated very securely ($P_{\rm ran} = 0.003$) with an $I = 17$ M2 V star displaying clear diffraction spikes in its WFPC2 image.

(xiii) *ISOHDFS J223251-603335.* This is identified with an $I = 22$ galaxy 3 arcsec away, yielding $P_{\rm ran} = 0.102$ for association with the EIS *K*-band catalogue. RGM, AF, MRR, Gwyn (1999) and the SUNY group estimate $z_{\rm ph} = 0.50$, 0.70, 0.95, 0.56 and 0.57, respectively, for this galaxy, the SED of which (with an adopted redshift of 0.7) shows the rise through the infrared characteristic of a starburst galaxy.

(xiv) *ISOHDFS J223252-603327.* This is a radio source (0.109 mJy at 1.4 GHz: A. Hopkins, private communication), located at the centre of quite an extended region of emission in both *ISO* bands. The source is associated ($P_{\rm ran} = 0.073$) with the EIS *K*-band catalogue. SEXTRACTOR stellarity indices exist for this object in *U*, *B*, *V*, *R*, *I*, *J*, *H* and *K* bands from the EIS catalogue, and vary from 0.48 in *U* to 0.97, indicating that the image is getting more point-like at longer wavelengths. This, together with the radio detection, suggests that this may be an obscured AGN, although Rigopoulou et al. (2001) do not report any strong AGN

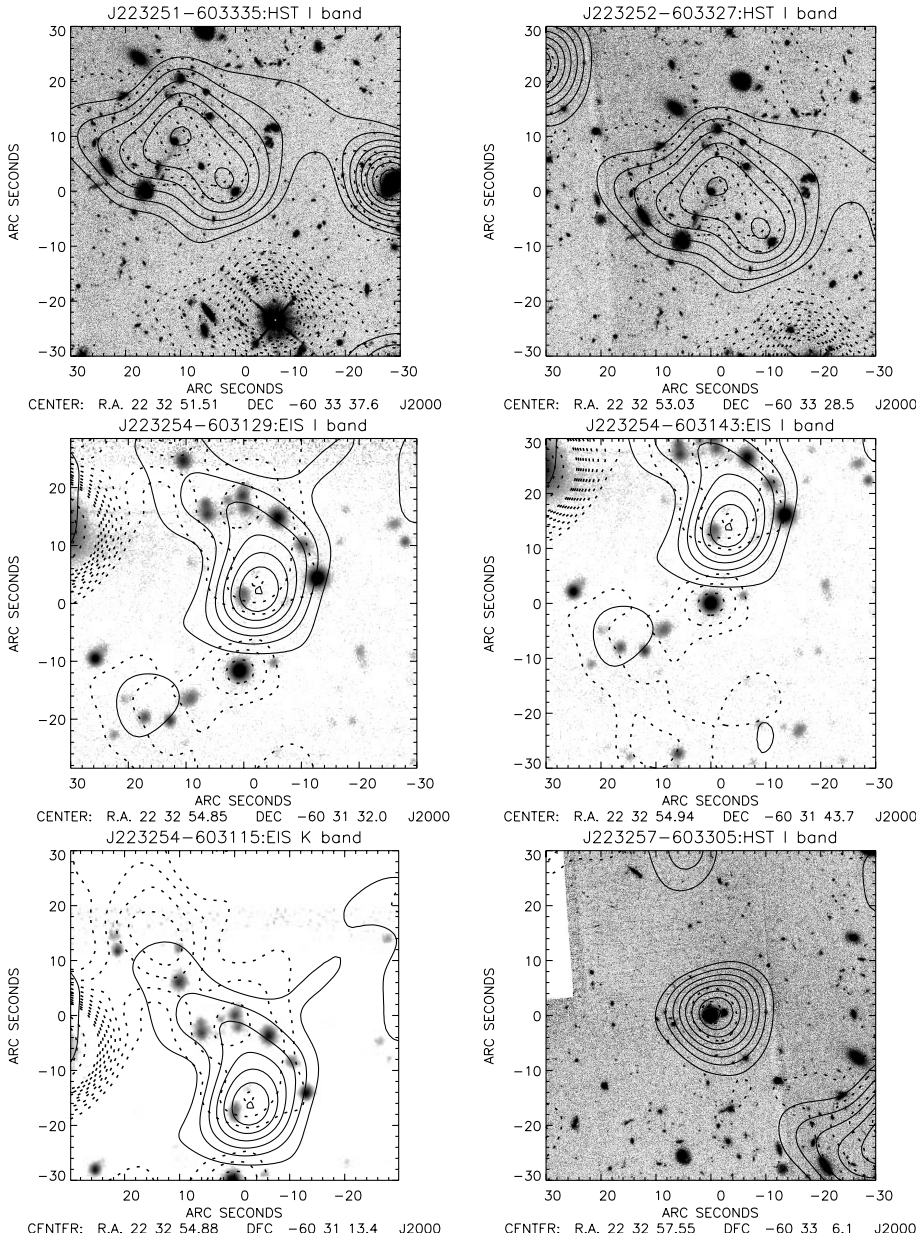

Figure 4 – *continued*

features in their spectrum of this object. That yielded $z = 1.27$, in excellent agreement with the photometric redshifts of Gwyn (1999) and the SUNY group (1.28 and 1.27, respectively), while RGM, AF and MRR obtain more widely varying values of 0.50, 0.90 and 1.46 for this galaxy.

(xv) *ISOHDFS J223254-603115.* This source, detected at both 6.7 and 15 μm, is associated with the brighter of a pair of very close (interacting?) galaxies separated by 2 arcsec. In the ESO EIS near-infrared catalogue of da Costa et al. (1998), the two galaxies have *J*, *H*, *K* magnitudes of 21.12, 20.64, 20.43 and 21.63, 21.18, 21.03, while the brighter galaxy has $I = 19.71$ in the GSFC CTIO catalogue, yielding $P_{\rm ran} = 0.044$, although it appears that the optical magnitudes include a significant contribution from the second galaxy, and as a result the optical photometry and near-infrared photometry in Fig. 6 (later) do not appear to be consistent. Fortunately, a spectroscopic redshift of $z = 0.5111$ was measured for this galaxy by Glazebrook et al. (in preparation), so it is not necessary to try to estimate a photometric redshift from this inconsistent set of magnitudes. Assuming that the near-infrared photometry is correct, the SED obtained using $z = 0.5111$ is very similar to that for the GRASIL model for the starburst galaxy NGC 6090.

(xvi) *ISOHDFS J223254-603129.* This is an intriguing case. The peaks of 6.7- and 15-μm emission are very close to each other, but 4–5 arcsec away (in directions 120° apart) from both an $I = 21$ galaxy (yielding $P_{\rm ran} = 0.162$) and a 0.143-mJy 1.4-GHz radio source, which appear not to be associated. It is possible that the *ISO* source is not associated with that galaxy either (but, instead, with an object too faint for these optical/near-infrared survey data that may or may not be the source of the radio emission), but we assume here that it is. RGM, MRR and AF estimate redshifts of 0.15, 0.48 and 0.50 for this galaxy, and adopting $z_{\rm phot} = 0.2$ we see, from Fig. 6 (later), that we obtain an SED similar to that of the GRASIL model for Arp 220.

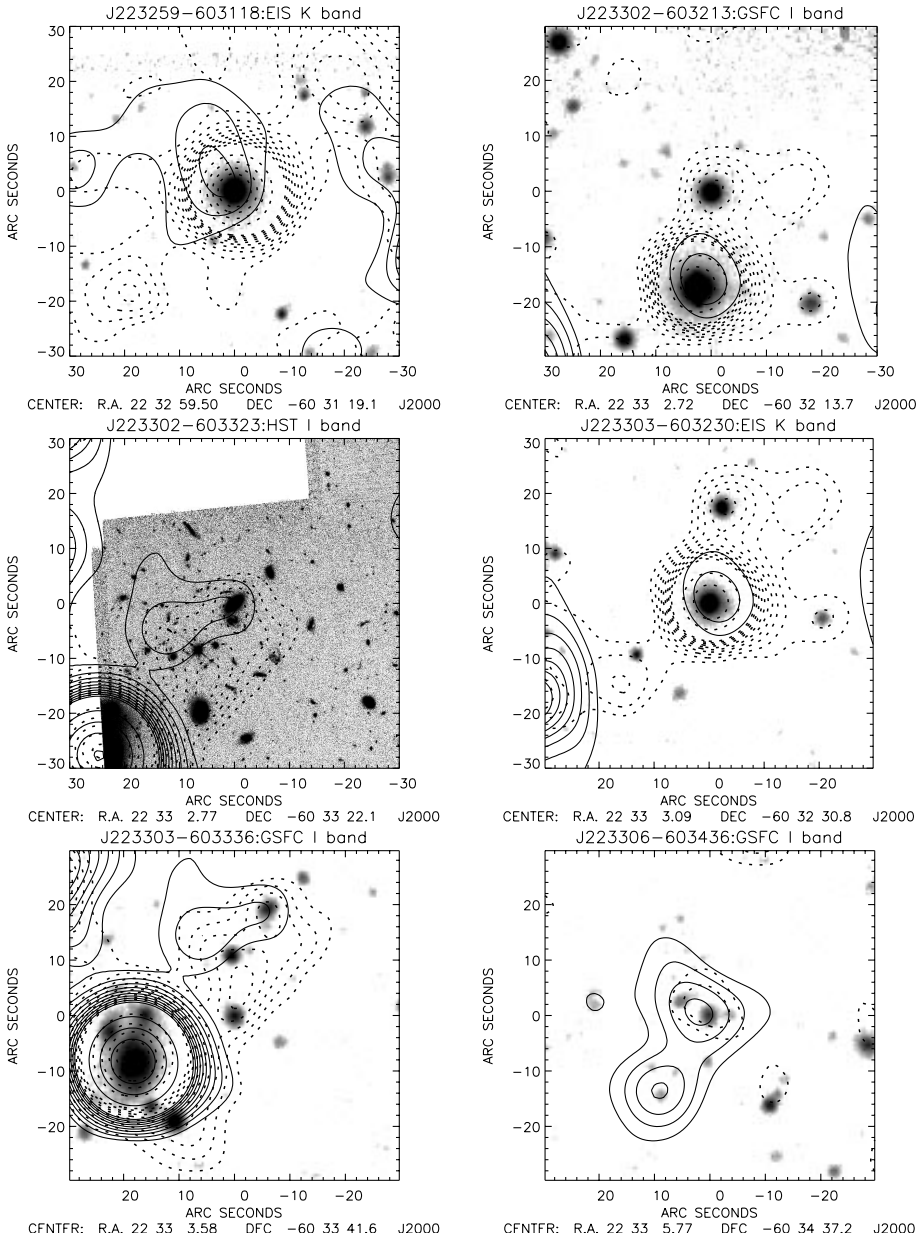

Figure 4 – *continued*

(xvii) *ISOHDFS J223254-603143.* This 6.7-μm source is associated securely ($P_{\rm ran} = 0.009$) with an $I = 18$ star, which shows clear diffraction spikes in *HST* imaging data.

(xviii) *ISOHDFS J223256-603059.* This 6.7-μm source has no reasonable association: its best association in the GSFC CTIO catalogue is with an $I = 22.5$ galaxy 5 arcsec away, yielding $P_{\rm ran} = 0.398$. The source is located very close to the very bright source ISOHDFS J223259-603118, and may be an artefact produced by inaccuracies in the application of our background subtraction procedure so close to this, the second brightest 6.7-μm source in our catalogue.

(xix) *ISOHDFS J223256-603513.* There is no reasonable association for this 15-μm source in the GSFC CTIO catalogue, which is the only one covering this area: the best association is with an $I = 22$ galaxy 7 arcsec away, which yields $P_{\rm ran} = 0.697$.

(xx) *ISOHDFS J223257-603305.* This 15-μm source is associated ($P_{\rm ran} = 0.047$) with an $I = 20$ galaxy for which Glazebrook et al. (in preparation) determined a redshift of $z = 0.5823$ from a spectrum exhibiting a number of narrow emission lines, which, together with the relative levels of the 15-μm detection and 6.7-μm upper limit, suggests that this is a starburst galaxy, although its SED is not a particularly good match to any of the GRASIL models. RGM, AF and MRR estimate $z_{\rm phot} = 0.40, 0.60$ and 0.62, respectively, for this source.

(xxi) *ISOHDFS J223259-603118.* This strong 6.7-μm source is a bright star, detected also at 15 μm but masked out of most of the SExtractor catalogues created from the optical/near-infrared surveys under discussion here. It appears in the EIS survey as a $K = 14$ G2 III star, yielding $P_{\rm ran} < 0.001$.

(xxii) *ISOHDFS J223302-603137.* Like ISOHDFS J223256-603059, this 6.7-μm source has no reasonable identification: the best candidate in the GSFC CTIO catalogue is a faint ($I = 25$) galaxy lying almost 5 arcsec away, and yielding $P_{\rm ran} = 0.539$. This source lies close to the bright star ISOHDFS J223259-603118, and,

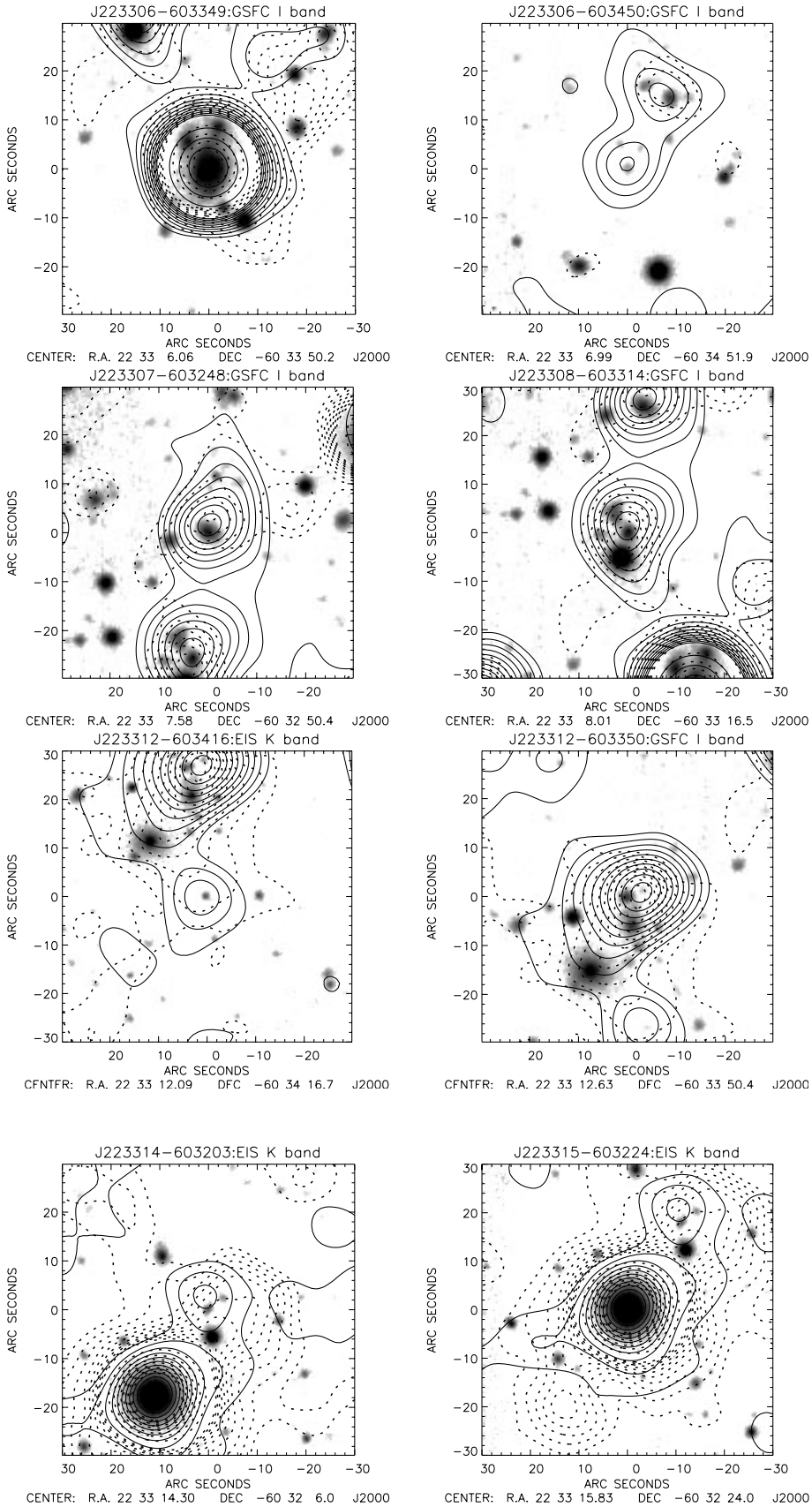

Figure 4 – *continued*

Table 1. Properties of the objects associated with the *ISO* sources in the HDF-S.

ISO Source	RA[a]	Dec.[b]	P_{ran}	*U*	*B*	*V*	*R*	*I*	*J*	*H*	*K*	*z*
J223237-603256	32 37.4	32 57.6	0.001	20.53	19.54	17.93	16.77	15.49				(0.00)
J223237-603235[c]	32 37.9	32 33.5	0.001	20.38	19.33	17.91	17.12	16.48				(0.00)
J223240-603141	32 40.6	31 43.6	0.095	22.88	22.82	22.09	21.19	20.46				(0.45)
J223243-603242	32 43.0	32 42.4	0.047	22.91	22.92	21.64	20.65	19.85	18.57	17.75	16.89	(0.50)
J223243-603441	32 43.5	34 42.3	0.021	21.60	21.71	20.56	19.63	18.94	17.71	16.83	16.14	(0.50)
J223243-603351	32 43.5	33 51.6	0.028	19.98	20.35	20.34	19.92	19.50	18.96	18.13	17.81	0.0918
J223244-603455	32 44.1	34 57.2	0.031	21.50	21.71	20.68	19.91	19.28	18.15	17.34	16.70	(0.35)
J223244-603110	32 44.3	31 11.4	0.066	22.08	22.13	21.43	20.74	20.23	19.70	19.03	18.26	0.25
J223245-603418	32 45.6	34 18.9	0.078	23.55	23.20	22.02	21.19	20.45	18.94	17.87	17.08	0.4606
J223245-603226	32 45.8	32 26.3	0.080	23.26	23.15	22.28	21.29	20.59	19.33	18.39	17.66	0.59
J223247-603335	32 47.7	33 35.9	0.030	21.99	22.06	21.06	20.03	19.24	17.97	17.01	16.31	0.5803
J223250-603359	32 50.5	34 00.8	0.003	21.44	20.32	18.78	17.78	16.75	15.53	14.83	14.63	(0.00)
J223251-603335	32 51.5	33 37.7	(0.102)	23.87	24.36	23.44	22.50	21.89	20.72	19.58	18.92	(0.56)
J223252-603327	32 53.0	33 28.6	(0.073)	24.91	24.80	24.10	23.33	22.37	20.60	19.57	18.96	1.27
J223254-603129	32 54.8	31 31.1	0.123	23.22	23.78	22.53	21.48	20.84	20.47	19.45	18.81	(0.20)
J223254-603143	32 54.9	31 44.1	0.009	23.39	21.92	20.36	19.22	18.02	16.62	15.87	15.65	(0.00)
J223254-603115[d]	32 54.8	31 14.6	0.044	23.52	23.22	21.73	20.51	19.67	20.23	19.26	18.57	0.5111
J223257-603305	32 57.5	33 06.0	0.047	21.87	22.09	21.44	20.66	20.01	19.00	18.09	17.45	0.5823
J223259-603118	(32 59.5	31 19.1)	(<0.001)						12.68	12.22	12.17	(0.00)
J223302-603213	33 02.7	32 13.8	0.006	22.76	21.52	19.94	18.78	17.46	16.01	15.38	15.15	0.00
J223302-603323	33 02.8	33 22.4	0.049	22.74	22.82	21.68	20.70	19.95	18.62	17.70	16.90	(0.60)
J223303-603230	(33 03.1	32 30.8)	(0.001)						14.08	13.35	13.18	0.00
J223303-603336	33 03.6	33 41.7	0.131	22.32	22.34	21.14	20.40	19.78	18.71	17.84	17.20	(0.35)
J223306-603436	33 05.8	34 37.2	0.095	24.37	23.93	22.55	21.34	20.44	19.00	17.89	17.08	(0.60)
J223306-603349	33 06.0	33 50.3	0.002	18.78	18.79	17.80	17.29	16.67	15.79	15.07	14.50	0.1733
J223306-603450	33 07.0	34 51.7	(0.094)	25.29	25.31	24.79	23.46	22.45	21.08	20.01	19.07	(0.75)
J223307-603248	33 07.6	32 50.3	0.034	22.20	22.20	21.18	20.21	19.54	18.37	17.43	16.73	0.513
J223308-603314	33 08.2	33 21.6	0.004	20.05	18.98	17.87	17.21	16.66	15.86	15.19	15.11	(0.50)
J223312-603416	(33 12.1	34 16.7)	(0.128)						21.57	20.38	19.34	(1.30)
J223312-603350	33 12.6	33 50.5	0.103	23.20	23.42	22.40	21.41	20.34	19.22	18.60	18.15	(0.50)
J223314-603203	(33 14.3	32 06.0)	(0.111)						20.77	19.68	18.98	(0.20)
J223315-603224	(33 15.8	32 34.0)	(<0.001)						11.58	10.86	10.67	0.00

Notes: The positions and P_{ran} values tabulated refer to the associated object in the GSFC catalogue, with the exception of the eight sources that have P_{ran} values in parentheses, which denote that they refer to the association with an object in the EIS near-infrared catalogue. For five of these cases (those with positions in parentheses) this is because the source is missing from the GSFC catalogue, while the remaining have significantly lower P_{ran} values resulting from their likelihood ratio association with the EIS *K*-band catalogue than with the GSFC *R*-band catalogue, as a result of red $R-K$ colours; these three objects are the first, second and ninth reddest of the 24 associated objects for which $R-K$ has been measured.

[a]All right ascensions prefixed by 22^h.

[b]All declinations prefixed by $-60°$.

[c]The object associated with this source is not included in the GSFC catalogue, so the tabulated photometric data come from the EIS catalogue of da Costa et al. (1998).

[d]The position of the object associated with this source in the GSFC catalogue suggests that the optical magnitudes quoted here may be too bright, through the inclusion of a close, faint companion, which the EIS near-infrared catalogue marks as a separate object, but which the GSFC catalogue does not.

like the other unidentified 6.7-μm source, ISOHDFS J223256-603059, may be an artefact resulting from background subtraction errors.

(xxiii) *ISOHDFS J223302-603213.* The object associated with this source is bright ($I = 17$) and less than 1 arcsec from the *ISO* position, yielding a P_{ran} value of 0.006. It is classed as stellar by SExtractor, and classified as an M3 V star on the basis of the spectrum taken by Glazebrook et al. (in preparation).

(xxiv) *ISOHDFS J223303-603230.* The association for this source, detected significantly at both 6.7 and 15 μm, is a bright object, spectroscopically confirmed to be an M1 V star using the Glazebrook et al. (in preparation) spectrum. It is masked out of the GSFC CTIO catalogue, but has $K = 15$ in the EIS near-infrared catalogue, yielding $P_{ran} = 0.001$.

(xxv) *ISOHDFS J223302-603323.* This source, detected in both bands, is associated ($P_{ran} = 0.049$) with an $I = 20$ galaxy for which RGM, AF, MRR, Gwyn (1999) and the SUNY group estimate photometric redshifts of 0.40, 0.60, 0.66, 0.474 and 0.400, respectively. With an adopted $z_{phot} = 0.60$, we obtain an SED similar to that of the GRASIL models for normal spirals like M100, NGC 6946 and M51.

(xxvi) *ISOHDFS J223303-603336.* The $I = 20$ galaxy associated with this source is 6 arcsec from the *ISO* position, which is the cause of its relatively poor P_{ran} value of 0.131, but the *ISO* source position could be shifted because of the close proximity of the bright source ISOHDFS J223306-603349 (the brightest in our 15-μm catalogue): once again, our background subtraction method could be leaving artefacts close to this bright source. RGM, AF, MRR, Gwyn (1999) and the SUNY group estimate photometric redshifts of 0.30, 0.35, 0.35, 0.419 and 0.440, respectively, for this galaxy, and with an adopted redshift of 0.35 we obtain an SED that fits the GRASIL starburst models well from the *U* band to 6.7 μm: we assume that the absence of a detection at 15 μm is due to problems with the subtraction of the side-lobes of ISOHDFS J223306-603349.

(xxvii) *ISOHDFS J223306-603349.* This $I = 16$ spiral galaxy, with a spectroscopic redshift determined by Glazebrook et al. (in preparation) to be $z = 0.1733$, is the brightest 15-μm source in our

catalogue, and has $P_{\rm ran} = 0.002$. It is detected in the radio at 0.533 and 0.300 mJy at 1.4 and 2.5 GHz, respectively (A. Hopkins, private communication), and, from Fig. 6 (later), we see that this galaxy has the SED of a normal spiral galaxy, rather than a starburst. RGM, AF and MRR estimate $z_{\rm phot} = 0.15, 0.25$ and 0.15, respectively, for this galaxy.

(xxviii) *ISOHDFS J223306-603436.* This $I = 20$ galaxy yields a $P_{\rm ran}$ value of 0.095, and is detected in both *ISO* bands. MRR, RGM and AF estimate photometric redshifts of 0.35, 0.60 and 1.00 for this galaxy, and an adopted $z_{\rm phot} = 0.60$ gives an SED very similar to that of the GRASIL models for the starburst galaxies M82 and NGC 6090.

(xxix) *ISOHDFS J223306-603450.* The identification of this source is complicated. Its *ISO* source position is less than 1 arcsec from a faint galaxy ($I = 22$), which is found with $K = 21$ in the EIS catalogue. The $P_{\rm ran}$ value resulting from the association of this object in the GSFC CTIO catalogue is 0.307, but it is a much better 0.094 when computed in the *K* band, indicating that this galaxy is very red in $R - K$. RGM, MRR and AF estimate redshifts for it of 0.65, 1.05 and 0.90, and with an adopted $z_{\rm phot} = 0.75$ we obtain an SED similar to the GRASIL model of Arp 220.

(xxx) *ISOHDFS J223307-603248.* This source, detected in both bands, is securely ($P_{\rm ran} = 0.034$) associated with an $I = 20$ galaxy for which Glazebrook et al. (in preparation) have determined a spectroscopic redshift of $z = 0.513$, yielding an SED similar to the GRASIL model for the starburst NGC 6090. RGM, AF and MRR estimate $z_{\rm phot} = 0.40, 0.50$ and 0.55, respectively, for this galaxy.

(xxxi) *ISOHDFS J223308-603314.* The likelihood ratio procedure associates (with $P_{\rm ran} = 0.034$) this source with an $I =$ 17 K4 V star, although the *ISO* contours in both bands are centred closer to an $I = 20$ galaxy 5 arcsec away. AF, MRR and RGM estimate redshifts of 0.05, 0.10 and 0.50, and we choose the last of these, as that gives the best fit to one of the GRASIL SEDs, that for the NGC 6090 model, but highlight that this is one of our most uncertain redshift estimates.

(xxxii) *ISOHDFS J223312-603350.* Detected significantly in both bands, this source is associated (with $P_{\rm ran} = 0.103$) with an $I = 20$ galaxy 2 arcsec from the 6.7-μm source position and 3 arcsec from that at 15-μm. Glazebrook et al. (in preparation) took a spectrum at this sky position, but it yielded no features capable of determining the redshift of the galaxy. RGM, AF and MRR determine photometric redshifts of 0.45, 0.70 and 0.32, respectively, but none of these yields an SED in particularly good agreement with the GRASIL starburst models: we adopt $z_{\rm phot} = 0.50$, as that gives, perhaps, the best agreement (with the Arp 220 SED), but note that this is highly uncertain.

(xxxiii) *ISOHDFS J223312-603416.* This *ISO* source position lies 1 arcsec from a faint ($K = 21$) EIS galaxy, which is not present in the GSFC CTIO catalogue. This near-infrared association yields $P_{\rm ran} = 0.128$, and MRR, AF and RGM estimate redshifts of 1.24, 1.30 and 2.05, respectively, although this is clearly very uncertain, since it is determined from *JHK* photometry alone. The relative fluxes in the two *ISO* and three near-infrared bands suggest that this is a starburst galaxy, but none of the estimated redshifts listed above results in a good fit to any of the GRASIL SED models; for definiteness we assume $z_{\rm phot} = 1.3$, but stress that this is not at all well-constrained.

(xxxiv) *ISOHDFS J223314-603203.* This is another example of a background subtraction artefact complicating the identification of a source. This source, detected significantly in both bands, lies close to a very bright star (the brightest 6.7-μm source in our catalogue, and the second brightest at 15 μm) and has no reliable association. The region is masked out of the GSFC CTIO catalogue, while the EIS near-infrared catalogue produces an association with $P_{\rm ran} = 0.111$ with a $K = 21$ galaxy 3 arcsec from the *ISO* source position, but the contours in this region have probably been disturbed by the background subtraction procedure. RGM and MRR estimate redshifts of 0.45 and 0.82, respectively, for this galaxy, on the basis of *JHK* photometry only, while we note that a significantly lower redshift of $z_{\rm phot} = 0.20$ produces a reasonable match to the SED of the starburst NGC 6090, so we adopt that here. It is clear, however, that this is one of our most uncertain associations.

(xxxv) *ISOHDFS J223315-603224.* This is the brightest source in our catalogue at 6.7 μm and the second brightest at 15 μm. It is a bright ($K = 13$) M2 V star, and is masked out of the GSFC CTIO catalogue, but its association with the EIS near-infrared catalogue yields $P_{\rm ran} < 0.001$.

In summary, we have found associations for 32 out of the 35 *ISO* sources from Paper I. Of the remaining three, two (ISOHDFS J223256-603059 and J223256-603137) were detected only at 6.7 μm and lie very close to sources that are very bright in that band, and which may well have compromised the background subtration procedure in that area, resulting in a false detection, or a significant shift in the source position. The third, ISOHDFS J223256-603513, was detected only at 15 μm, and is a peak in an extended region of emission stretching from a bright source just below the southern boundary of our source detection region (see fig. 6 of Paper I). Eight of the 32 identified sources are stars, leaving a total of 24 galaxies to be considered further.

3 STAR FORMATION RATE ESTIMATORS

In this section we discuss and compare the various methods by which we might estimate the SFRs of our *ISO* sources.

3.1 Methods for estimating star formation rates

A multitude of methods have been advocated for the estimation of the SFRs of galaxies, and, as discussed for example by Cram et al. (1998) and Granato et al. (2000), they agree to varying degrees. All attempt to detect the observational consequences of the formation of massive stars, and then use a model for the stellar IMF to infer the total rate of formation of stellar mass. This inevitably introduces some uncertainty into the SFR estimates, owing to the assumption of a universal IMF for all galaxies and the lack of a clear choice between competing models for it. More serious is the fact that the formation of massive stars in external galaxies, like that in our own Galaxy, is expected to take place in giant molecular clouds, enshrouded by dust, and, as argued for example by Silva et al. (1998) and Jimenez et al. (1999), the resultant emission from the star-forming region cannot be well represented by a simple model such as a dust-screen in front of a dust-free starburst.

Despite these difficulties, there are several well-used prescriptions for estimating the SFRs of galaxies on the basis of simple broad-band fluxes, as these are, typically, all that are available for the large samples of galaxies used in censuses of the cosmic star formation history. The first of these is to use the *U*-band magnitude, arguing that the ultraviolet emission comes principally from massive, young stars. There are two problems with this. First, the *U* band ($\lambda_{\rm eff} = 365$ nm) is not far enough into the ultraviolet for the emission from older stars to be negligible, but it is possible to correct for this effect, by using model spectra to bootstrap from the

U band to, say, 250 nm, where the emission is dominated by massive stars. Cram et al. (1998) do this, obtaining the following relationship between the U-band luminosity of a galaxy and its rate of massive ($M \geq 5\,\mathrm{M}_\odot$) star formation:

$$\frac{SFR(M \geq 5\,\mathrm{M}_\odot)}{\mathrm{M}_\odot\ \mathrm{yr}^{-1}} = \frac{L_\nu(U)}{1.5 \times 10^{22}\,\mathrm{W\,Hz}^{-1}}, \quad (2)$$

for an assumed $\psi(M) \propto M^{-2.5}$ IMF running from 0.1 to 100 $\mathrm{M}_\odot$. An obvious objection to this is that it fails to account for the effects of dust in the star-forming galaxies, especially in the case that more massive starbursts are dustier. The recent models of Devriendt, Guiderdoni & Sadat (1999) seek to model the SEDs of dusty starbursts from the ultraviolet to the submillimetre in a self-consistent fashion, taking account of the absorption of ultraviolet light from massive young stars by the dust surrounding them, and its use in heating up the dust, leading to emission in the far-infrared and submillimetre. Their models yield the following correlations between the SFR (for a Salpeter 1955 IMF over [0.1,120] $\mathrm{M}_\odot$) and the luminosities at two ultraviolet wavelengths:

$$\frac{SFR}{\mathrm{M}_\odot\ \mathrm{yr}^{-1}} = \left[\frac{\lambda L_\lambda(280\,\mathrm{nm})}{7.7 \times 10^{34}\,\mathrm{W}}\right]^{1.62} \quad (3)$$

and

$$\frac{SFR}{\mathrm{M}_\odot\ \mathrm{yr}^{-1}} = \left[\frac{\lambda L_\lambda(160\,\mathrm{nm})}{9.2 \times 10^{34}\,\mathrm{W}}\right]^{1.72}. \quad (4)$$

Devriendt et al. (1999) caution against the over-interpretation of these best-fitting correlations (about which their model galaxies scatter quite widely), but the non-linearity of the relationships that they describe between SFR and ultraviolet luminosity is qualitatively what would be expected in a model in which the more massive a starburst is the dustier it is, and suggests that this effect may be corrected for, albeit crudely.

The bolometric luminosities of luminous starburst galaxies are dominated by thermal emission from dust in the far-infrared. In general, this emission is a combination of extended ('cirrus') emission from dust heated by the ambient interstellar radiation field, more localized 'starburst' emission from the dust in regions of massive star formation heated by the ultraviolet flux from O and B stars, and, possibly, 'AGN' emission from the hot dusty torus of an active galactic nucleus. The relative importance of these components varies between galaxies (e.g. Rowan-Robinson & Crawford 1989), with the cirrus component declining to higher luminosities, where ultraluminous infrared galaxies (ULIRGs) are seen to be mostly fuelled by starburst emission, although some do have a dominant AGN component (Genzel et al. 1998): such simple modelling must be supplemented by consideration of emission from polycyclic aromatic hydrocarbons (PAHs) and inclusion of starburst components of different ages (Silva et al. 1998; Efstathiou, Rowan-Robinson & Siebenmorgen 2000) to fit the detailed SEDs revealed (e.g. Acosta-Pulido et al. 1996) by recent *ISO* spectroscopy. Various attempts have been made to relate this far-infrared emission to the amount of ultraviolet light that must be absorbed by dust to produce it, by which route the SFR of a galaxy (or, at least, the rate of formation of stars the light of which is obscured by dust) can be estimated from its far-infrared luminosity. Rowan-Robinson et al. (1997) summarized previous work on this method in the relationship

$$\frac{SFR}{\mathrm{M}_\odot\ \mathrm{yr}^{-1}} = \frac{\lambda L_\lambda(60\,\mu\mathrm{m})}{1.5 \times 10^{36}\,\mathrm{W}} \left(\frac{\phi}{\epsilon}\right), \quad (5)$$

where $\epsilon \simeq 1$ is the fraction of the (νL_ν) ultraviolet luminosity of the starburst that is re-emitted in the far-infrared, while $\phi \sim O(1)$ is a factor the deviation of which from unity can account for variations of the IMF from the standard Salpeter (1955) $\psi(M) \propto M^{-2.35}$ form over the range 0.1 to 100 $\mathrm{M}_\odot$: for example, it should be 3.3 if a Miller–Scalo (Miller & Scalo 1979) IMF is preferred, and 1/3.1 if the starburst forms only stars with $M > 1.6\,\mathrm{M}_\odot$. Cram et al. (1998) presented a similar relationship (based on the ideas of Condon 1992), which reads

$$\frac{SFR(M \geq 5\,\mathrm{M}_\odot)}{\mathrm{M}_\odot\ \mathrm{yr}^{-1}} = \frac{L_\nu(60\,\mu\mathrm{m})}{5.1 \times 10^{23}\,\mathrm{W\,Hz}^{-1}}, \quad (6)$$

assuming the same $\psi(M) \propto M^{-2.5}$ as in equation (2).

Similar expressions can be derived in terms of the integrated far-infrared/submillimetre emission. For example, the models of Devriendt et al. (1999) yield [for the same IMF as in equations (3) and (4)] the relationship

$$\frac{SFR}{\mathrm{M}_\odot\ \mathrm{yr}^{-1}} = \left[\frac{L_{\mathrm{IR}}(3-1000\,\mu\mathrm{m})}{3.0 \times 10^{36}\,\mathrm{W}}\right]^{1.05} \quad (7)$$

[cf. equations (3) and (4) where the power-law index deviates significantly from unity].

As reviewed by Condon (1992), there is a well-known correlation between the far-infrared and decimetric radio luminosities of actively star-forming galaxies, which is thought to arise from the fact that the bulk of the radio luminosity is produced by synchrotron emission from relativistic electrons spiralling in the remnants of supernovae originating in the same population of massive stars that produce the starburst component to the far-infrared luminosity. Since the cirrus component to the far-infrared luminosity is not expected to have associated radio emission, it has been argued that the decimetric radio luminosity of a starburst galaxy may provide the cleanest handle on its star formation rate, and Cram et al. (1998) present the following form for that relationship (assuming the same IMF as before):

$$\frac{SFR(M \geq 5\,\mathrm{M}_\odot)}{\mathrm{M}_\odot\ \mathrm{yr}^{-1}} = \frac{L_\nu(1.4\,\mathrm{GHz})}{4.0 \times 10^{21}\,\mathrm{W\,Hz}^{-1}}, \quad (8)$$

where, as before, Cram et al. consider only the formation of stars with $5 \leq M \leq 100\,\mathrm{M}_\odot$ in an $M^{-2.5}$ IMF. Additional SFR estimators exist, for example using the luminosity in the Hα line (e.g. Kennicutt 1998), but these, too, are affected by dust, as shown by Rigopoulou et al. (2001) on the basis of near-infrared VLT–ISAAC spectroscopy of the Hα line in a subsample of the *ISO* HDF-S objects considered here.

3.2 Comparing star formation estimates

It is natural to enquire how these SFR estimators compare, and this question was addressed empirically by Cram et al. (1998), using a somewhat heterogeneous compilation of data (U-band magnitudes, Hα, 60-μm and 1.4-GHz radio fluxes) from a variety of sources. They found that the SFRs deduced from the integrated far-infrared and decimetric radio luminosities are well correlated over more than four orders of magnitude, but that significant deviations from linearity and greater scatter are seen for the relationships between the SFRs deduced from the 1.4-GHz power and those from Hα and U-band luminosities. Some observational effects (e.g. slit losses in Hα spectroscopy) may be contributing to these trends, but they are consistent with the qualitative expectations of the picture outlined above in which massive stars are formed in dusty environments,

and reinforce the belief that this is the dominant mode of star formation in actively star-forming galaxies.

Here we perform a complementary study, which attempts to circumvent the observational problems that inevitably affect the analysis of any heterogeneous data sample drawn from many sources in the literature, by asking how these different star formation estimators fare when applied to model SEDs for a range of types of star-forming galaxy. To do this we use the GRASIL models of Silva et al. (1998), which provide good fits to the ultraviolet–radio SEDs of six nearby galaxies, namely three starburst galaxies (Arp 220, M82 and NGC 6090) with differing levels of activity, and three local spirals (M100, M51 and NGC 6946); similar models of starbursts are presented by Efstathiou et al. (2000), but they do not consider normal spirals, which is why we use the GRASIL models here. We refer the reader to the paper by Silva et al. (1998) for a discussion of the ultraviolet–millimetre SEDs, and to Silva (1999) for details of their extension into the radio, through consideration of separate thermal and non-thermal components to the radio emission, and note that Granato et al. (2000) have also compared star formation estimators through their application to GRASIL SEDs.

Silva et al. (1998) quote the SFR value (averaged over the previous 5×10^7 yr) corresponding to each SED model, for an assumed Salpeter (1955) IMF running from 0.1 to 100 $M_\odot$. Hence, to compare the SFR estimators, by seeing how well each recovers those values, we must scale equations (2)–(8) as required for them all to give the rate at which stellar mass would form given that reference IMF; this is analogous to the choice of the value of ϕ in the formalism of Rowan-Robinson et al. (1997). The derivation of the correct scaling factor in each case requires consideration of the model through which the particular observed luminosity is related to the rate of formation of massive stars: in equations (2), (3) and (4) the value of a particular monochromatic ultraviolet luminosity is used as a direct tracer of these stars; underlying equations (5), (6) and (7) is an assumption that some large ($\simeq 1$) fraction of their bolometric luminosity emerges [on a time-scale of $\sim O(10^6\,\mathrm{yr})$] in the far-infrared, owing to the reprocessing by dust; and the method of equation (8) relates the number of high-mass stars that become Type Ib and Type II supernovae to the synchrotron emission produced by their remnants.

In Appendix A, we show how each of these physical models yields a scaling to be applied to equations (2)–(8) to convert them to predictions for $\dot{M}$, the rate of formation of stellar mass, given our canonical IMF, which is a Salpeter (1955) IMF running from 0.1 to

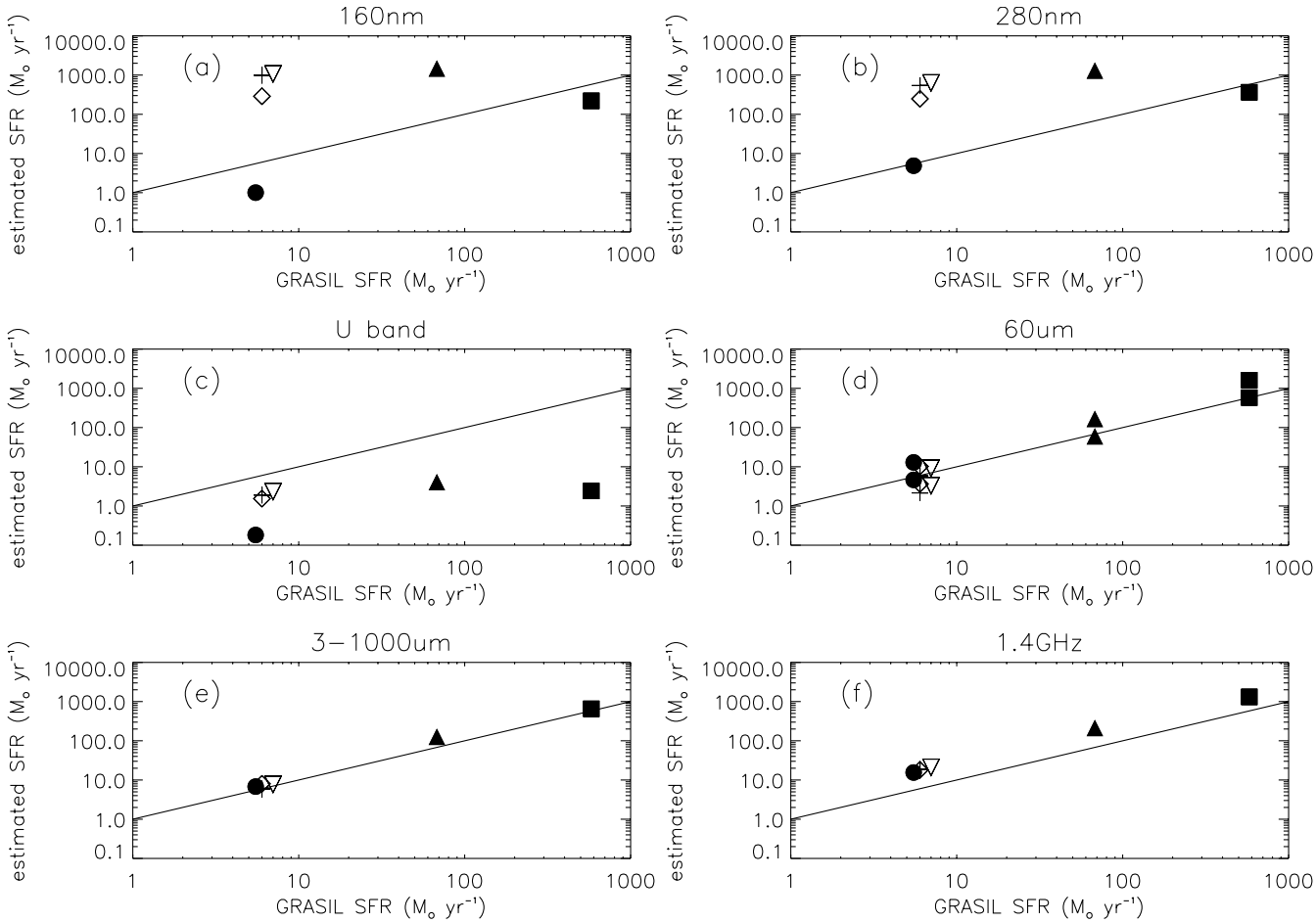

Figure 5. Comparison of the results of applying to GRASIL model SEDs six SFR estimation methods from equation (9), namely those based on: (a) the 160-nm luminosity, from Devriendt et al. (1999); (b) the 280-nm luminosity, from Devriendt et al. (1999); (c) the *U*-band luminosity, from Cram et al. (1998); (d) the 60-μm luminosity, from Cram et al. (1998) and Rowan-Robinson et al. (1997), denoted by the upper and lower sets of points, respectively; (e) the 3–1000 μm integrated luminosity, from Devriendt et al. (1999); (f) the 1.4-GHz luminosity, from Cram et al. (1998). For each method we plot the SFR estimate obtained by its application to the GRASIL SED models for M100 (inverted triangle), M51 (diamond), NGC 6946 (plus sign), NGC 6090 (filled triangle), M82 (filled circle) and Arp 220 (filled square) against the corresponding SFR value computed within the GRASIL model itself.

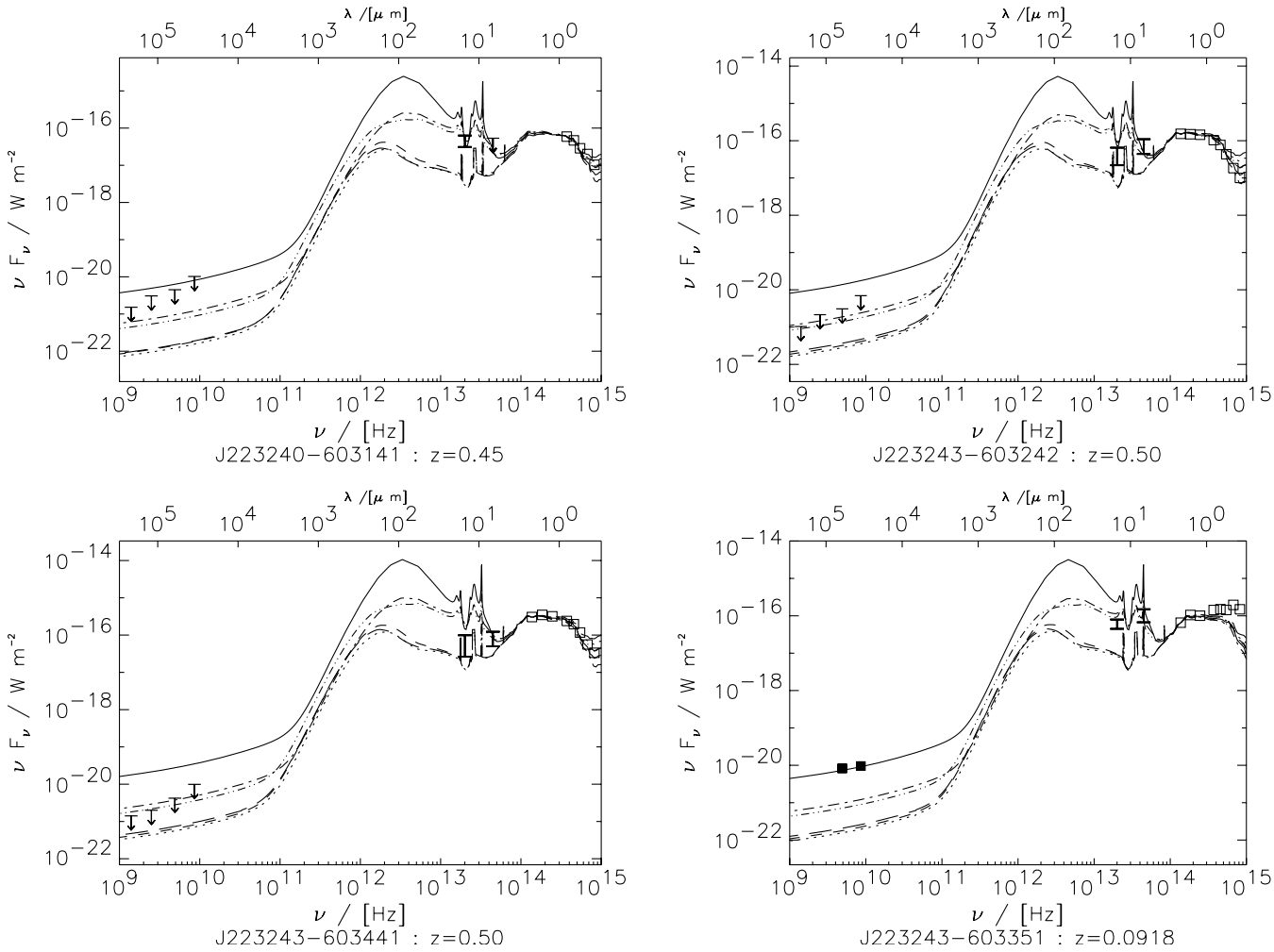

Figure 6. Spectral energy distributions for the 24 objects from Table 1 identified as galaxies. The squares mark the ultraviolet/optical/near-infrared and radio photometric data for the objects, from Table 1, while the solid, dotted, dashed, dash-dotted, dash–double-dotted and long-dashed lines show, respectively, the GRASIL model fits to the SEDs of Arp 220, M100, M51, M82, NGC 6090 and NGC 6946, redshifted as appropriate for each galaxy. The *ISO* data from table 8 of Paper I are plotted as error bars or upper limits, as appropriate.

$100\,\mathrm{M}_\odot$, in our canonical cosmology, which is an Einstein–de Sitter universe with a Hubble constant of $50\,\mathrm{km\,s^{-1}\,Mpc^{-1}}$. We find the following set of corrected versions of the estimators of equations (2)–(8):

$$\frac{\dot{M}}{\mathrm{M}_\odot\,\mathrm{yr}^{-1}} = \begin{cases} L_\nu(U)/2.6\times10^{21}\,\mathrm{W\,Hz^{-1}} \\ [\lambda L_\lambda(280\,\mathrm{nm})/7.0\times10^{34}\,\mathrm{W}]^{1.62} \\ [\lambda L_\lambda(160\,\mathrm{nm})/8.4\times10^{34}\,\mathrm{W}]^{1.72} \\ \lambda L_\lambda(60\,\mu\mathrm{m})/1.5\times10^{36}\,\mathrm{W} \\ L_\nu(60\,\mu\mathrm{m})/1.1\times10^{23}\,\mathrm{W\,Hz^{-1}} \\ [L_{\mathrm{IR}}(3-1000\,\mu\mathrm{m})/2.3\times10^{36}\,\mathrm{W}]^{1.05} \\ L_\nu(1.4\,\mathrm{GHz})/6.9\times10^{20}\,\mathrm{W\,Hz^{-1}}. \end{cases} \quad (9)$$

Having made these various scalings, we are ready to compare the SFR values obtained by applying the estimators of equation (9) to the six GRASIL SEDs with the values given for them by Silva et al. (1998), as shown in Fig. 5: note that the results from the two 60-μm-based estimators are plotted together. The first thing to note from this figure is that the far-infrared and radio estimators do far better at recovering the GRASIL SFRs than do the three ultraviolet-based ones. The integrated far-infrared estimator of Devriendt et al. (1999) is the closest to the GRASIL SFR value for all models, while the 1.4-GHz value is offset by a fairly constant factor of ∼3, indicating that, while there may be a problem with its absolute normalization (possibly caused by the way that the GRASIL SEDs are extended into the radio), this method works well for all the SED types considered, yielding accurate relative SFR values for them. The 60-μm-based estimators fare quite well, too, although the ratios of their SFR values to those from the GRASIL code are higher for starbursts (filled symbols) than for normal galaxies (empty symbols), suggesting that a far-infrared colour term should be included in the relationship between SFR and far-infrared luminosity.

The three ultraviolet-based estimators display a much more complex behaviour across the range of galaxy types. The *U*-band luminosity always gives a lower SFR estimate than the four integrated/far-infrared and radio estimators, and the discrepancy is appreciably larger for the starbursts than for the normal spirals, as expected if the ultraviolet light is generated in dustier environments in starbursts than in normal spirals. The two non-linear ultraviolet–SFR relations deduced by Devriendt et al. (1999) appear to over-estimate the SFRs of the spirals, and one of the

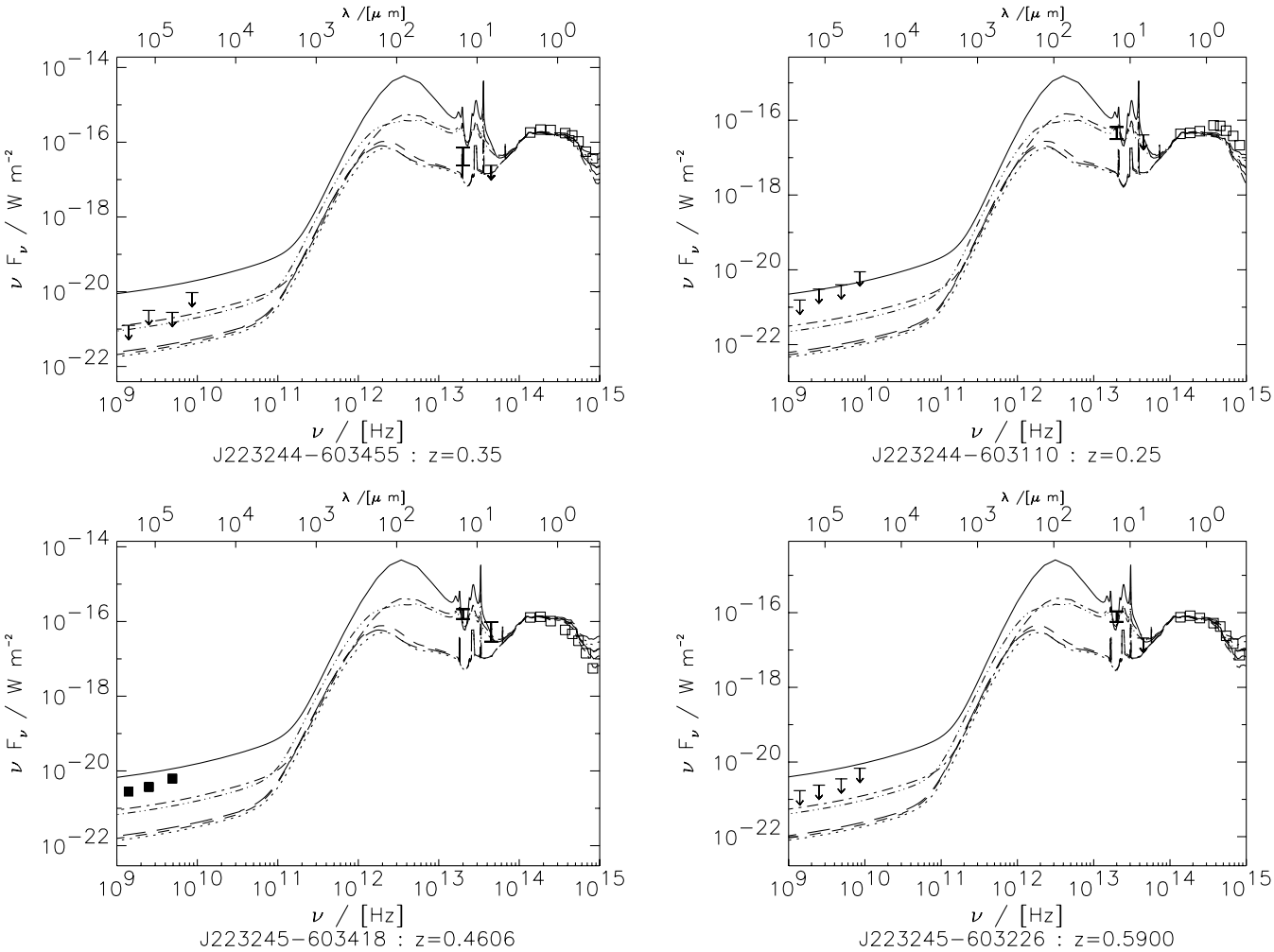

Figure 6 – *continued*

starbursts (NGC 6090), but do reasonably well for M82 and, especially, Arp 220. This could be because the Devriendt et al. (1999) models, although spanning the full range of galaxy types from inactive spirals to ULIRGs, are more directed at the understanding of starbursts and/or could simply reflect that the best-fitting correlations yielding equations (3) and (4) do not express anything physical in the models.

It is clear from these results that caution must be exercised in comparing SFRs in the literature, which might have been made using different estimators and with differing assumptions as to the stellar IMF and the exact specification of the astrophysical model underlying their application. Even when scaled to a common reference IMF, the SFR estimators based on far-infrared or radio luminosities are only consistent to within a factor of 2, while the ultraviolet-based ones are seen to be far less secure. The consistency between the ratios of SFR values obtained by the four radio- and integrated/far-infrared-based estimators across the six SEDs is, of course, simply a manifestation of the universality of the radio–far-infrared correlation (reviewed by Condon 1992), but our results do afford some confidence that they are measuring quantities correlated with the 'true' SFR, at least to the extent that is well reproduced by the GRASIL models, which cannot be said for the ultraviolet-based estimators. On the basis of these results, the integrated infrared luminosity appears to be the best SFR estimator out of the set we have investigated, so it is that which we shall use in what follows, when we deduce SFR values for our *ISO* sources.

4 SPECTRAL ENERGY DISTRIBUTIONS AND STAR FORMATION RATES OF *ISO* HDF-S SOURCES

In this section we estimate SFRs for our *ISO* sources, through the application of the integrated infrared luminosity estimator judged to be the best in Section 3.2 to GRASIL model SEDs fitted to the photometric data for each of the 24 galaxies given in Table 1, plus radio data (mostly upper limits) kindly provided in advance of publication by the ATNF HDF-S survey team (A. Hopkins, private communication). We do not expect our *ISO* sources to match exactly one of the six GRASIL models, but, to the extent that the models span the range of SEDs of star-forming galaxies likely to feature in our mid-infrared survey, this method gives us a handle on the uncertainty in the deduced SFR value of each *ISO* source resulting from uncertainty in its true SED: note that the SEDs of the three normal spirals are very similar, and it is only when an appreciable starburst component kicks in that the shape of the SED begins to change significantly. To facilitate the choice of the GRASIL model most appropriate to each galaxy, we plot in Fig. 6 the photometric data set for each source, together with the six

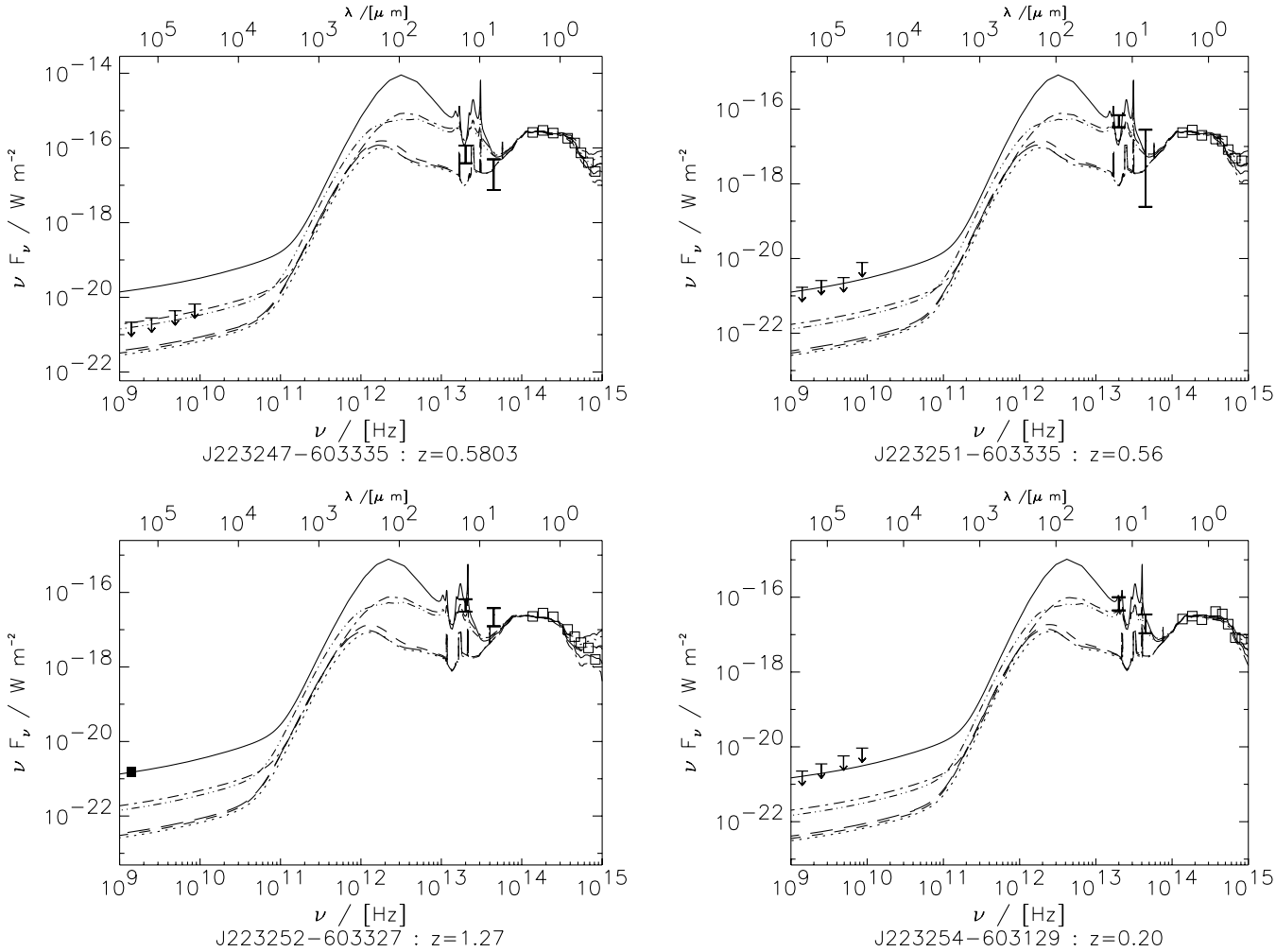

Figure 6 – *continued*

model SEDs, normalized in each case to match the *K*-band magnitude of the galaxy associated with the *ISO* HDF-S source, or the *I*-band magnitude in the one case (J223240-603141) of a galaxy lying outside the region of the EIS *K*-band survey. From this figure we conclude the following about the SFRs of the 24 *ISO* HDF-S galaxies.

(i) *ISOHDFS J223240-603141.* The observed *I*-band to 15-μm colour suggests that this is a starburst galaxy, rather than a normal spiral dominated by cirrus emission: the lack of a detection at 7 μm is just consistent with that, and J223240-603141 does lie close to a very bright 7-μm source, so it is possible that its 7-μm flux estimate has been corrupted by the subtraction of the negative lobes of the bright source. The lack of detections at 1.4, 2.5 and 4.9 GHz argues against the starburst being as extreme as that in Arp 220, and the optical colours favour an SED like that of NGC 6090 over that of M82. Using the 1.4-GHz, 60-μm (Cram et al. 1998), 60-μm (Rowan-Robinson et al. 1997, with $\epsilon = \phi = 1$), and 3–1000 μm prescriptions we obtain SFR estimates of 43, 34, 12 and $20\,M_\odot\,yr^{-1}$, respectively, from adopting this SED. On the basis of Section 3.2, we adopt the last of these, so our best estimate of the true SFR for this galaxy is $20\,M_\odot\,yr^{-1}$.

(ii) *ISOHDFS J223243-603242.* This is a slightly ambiguous case. The optical/near-infrared colours of this galaxy fit the M82 model SED very well, as does the 7-μm flux, once the model has been normalized to the observed *K*-band flux of J223243-603242; however, the 15-μm flux seems a little low and the lack of a 1.4-GHz detection is marginally inconsistent with the M82 model. Using the M82 model SED, the same four SFR estimators give 145, 121, 43 and $60\,M_\odot\,yr^{-1}$, while, if we had adopted an M100 SED instead, we would have obtained values of 22, 9, 3 and $7\,M_\odot\,yr^{-1}$, respectively. The M82 SED is a better fit overall, so we adopt a best-guess SFR value for this galaxy of $60\,M_\odot\,yr^{-1}$, noting that, while the precise SFR value is uncertain, it is clear this galaxy is forming stars at a rate of several tens of $M_\odot\,yr^{-1}$.

(iii) *ISOHDFS J223243-603351.* This is one of the four *ISO* HDF-S sources detected in the radio and the strength of these detections (at 4.9 and 8.6 GHz), together with the optical/near-infrared SED of the galaxy, which rises into the ultraviolet, suggests that this may be an AGN, and this is confirmed by the presence of a broad line in its optical spectrum: we therefore do not estimate the SFR in this source.

(iv) *ISOHDFS J223243-603441.* This is a second source, like J223243-603242, that has an optical/near-infrared SED well matching the starburst models, but *ISO* fluxes which do not unambiguously support that interpretation, as the 15-μm flux is lower than would be expected for a starburst on the basis of its SED up to 6.7 μm. From Fig. 4 we see that this source is close to a much

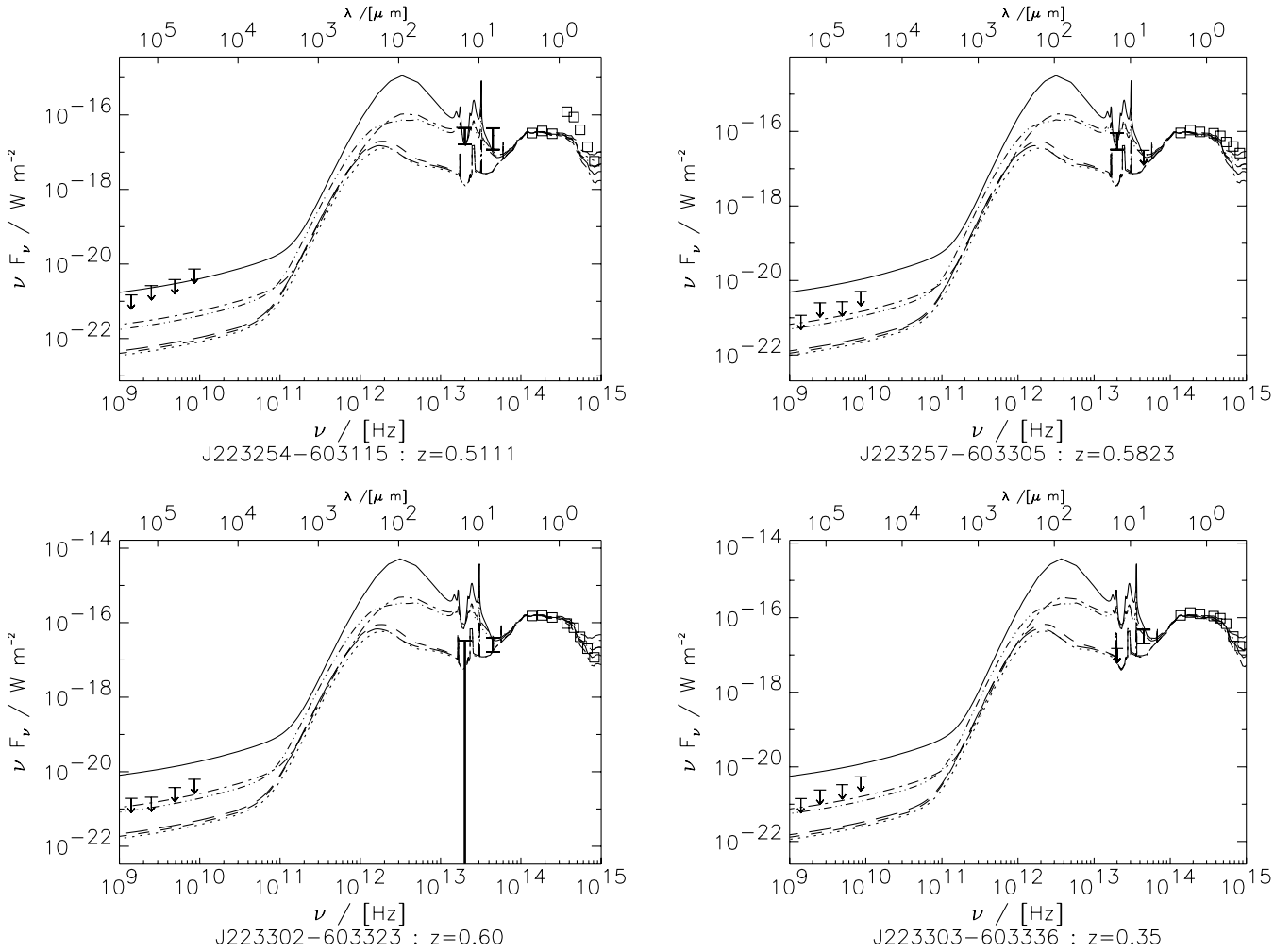

Figure 6 – *continued*

brighter source at 15 μm, so it is possible that its flux in that band has been under-estimated, owing to the difficulty of subtracting the negative lobe from the brighter source. If we assume that, and adopt an NGC 6090 SED, then we obtain SFR values of 216, 169, 61 and 108 $M_\odot\,yr^{-1}$ from the usual four estimators, while, if we take the 6.7–15 μm colour at face value, favouring an M51 SED, we obtain, instead, values of 49, 28, 10 and 19 $M_\odot\,yr^{-1}$. As a compromise, we adopt a best guess of 50 $M_\odot\,yr^{-1}$, but note that is uncertain by a factor of 2, at least.

(v) *ISOHDFS J223244-603110.* The optical to near-infrared SED of this galaxy is a little unusual, suggesting a mismatch in the apertures used to measure the optical and near-infrared magnitudes. Fixing the model SEDs to match the *K*-band magnitude, we obtain a good fit to the M82 and NGC 6090 models, yielding an SFR estimate of 4 $M_\odot\,yr^{-1}$ from applying the integrated infrared luminosity estimator to the fitted M82 SED mode, so this is not a very strong starburst.

(vi) *ISOHDFS J223244-603455.* The proximity of a brighter 7-μm source might explain the lack of a detection in that band, owing to the lobe-subtraction problem, but it seems more likely, on all evidence, that this is a normal spiral and not a starburst. Using the NGC6946 model SED the integrated L_{IR} estimator yields 4 $M_\odot\,yr^{-1}$, a modest SFR, consistent with this interpretation.

(vii) *ISOHDFS J223245-603226.* Again, the lack of a 7-μm detection slightly confuses an otherwise fairly confident identification of this with an M82- or NGC 6090-type starburst, and, once more, this source is close to a strong 7-μm source, so this may be due to the lobe-subtraction problem. If we adopt the NGC 6090 SED model, which gives a slightly better fit to the optical/near-infrared SED, we obtain a best-guess SFR of 36 $M_\odot\,yr^{-1}$ for this galaxy.

(viii) *ISOHDFS J223245-603418.* This is one of the most unambiguous starburst detections. Its ultraviolet–15 μm colours are well fitted by the M82 SED (and almost as well by the Arp 220 model), but the solid radio detections at 1.4, 2.5 and 4.9 GHz suggest a starburst stronger than M82. Using the M82 and Arp 220 SEDs we obtain SFRs of 40 and 300 $M_\odot\,yr^{-1}$, using the integrated L_{IR} estimator, confirming that this is a powerful starburst, although leaving some doubt as to its true SFR: we adopt a best guess of 100 $M_\odot\,yr^{-1}$, but note that this is uncertain by a factor of 2, at least.

(ix) *ISOHDFS J223247-603335.* Another case where an unambiguous discrimination between spiral and starburst is difficult: the *ISO* fluxes are a little lower than expected for the starburst fit to the optical/near-infrared SED. Taking the NGC 6090 and M100 SEDs, which bracket the data points, we obtain SFRs of 130 and 16 $M_\odot\,yr^{-1}$, from application of the integrated L_{IR} estimator, so there is quite some uncertainty in the SFR for the source: we adopt a value of 50 $M_\odot\,yr^{-1}$, again with a factor of 2

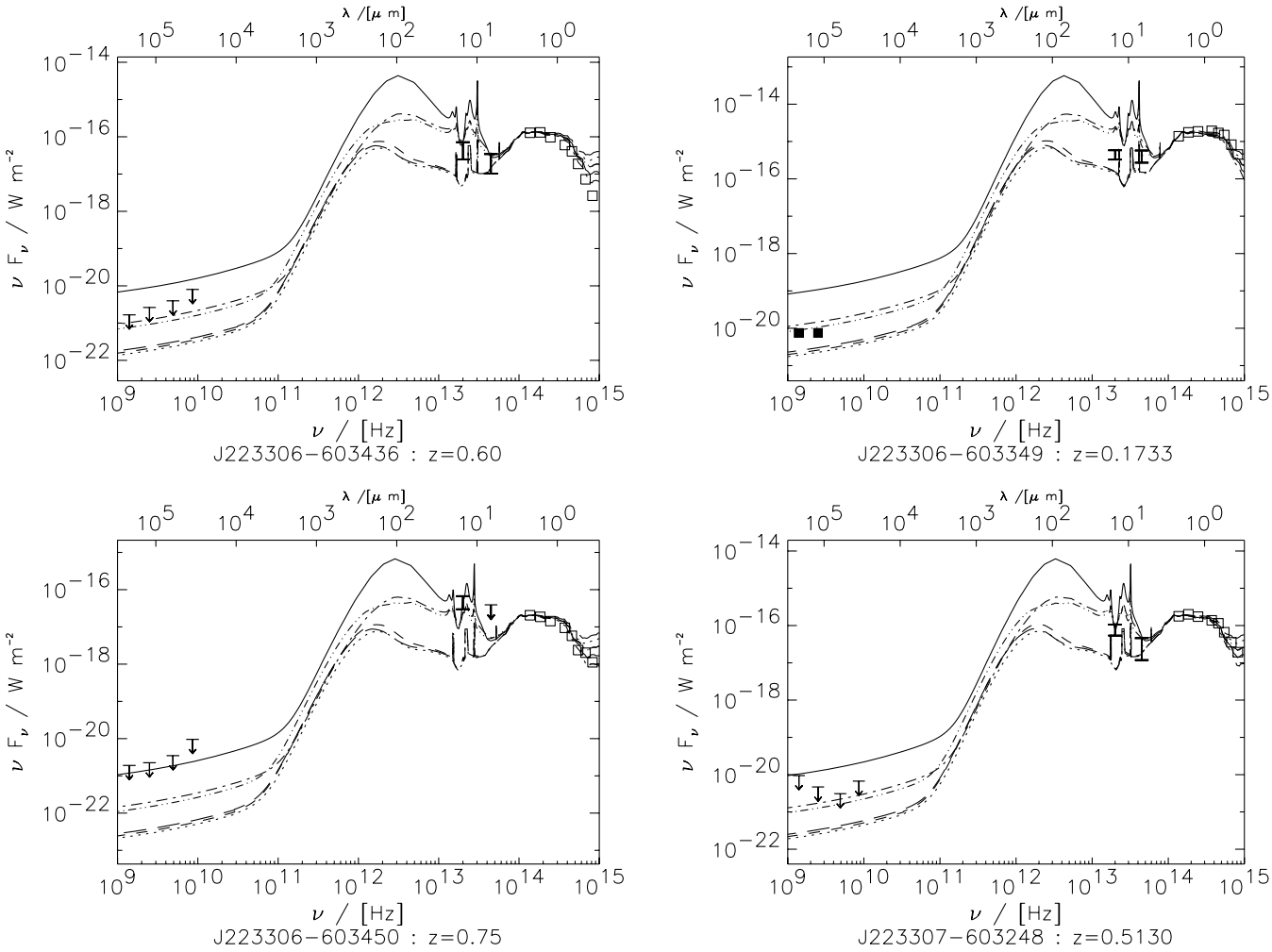

Figure 6 – *continued*

uncertainty, at least, although it is clear that this galaxy is definitely forming stars actively.

(x) *ISOHDFS J223251-603335.* The SED of this source is quite well fitted by the NGC 6090 model, with which the integrated $L_{\rm IR}$ estimator yields an SFR estimate of $10\,{\rm M}_{\odot}\,{\rm yr}^{-1}$, so it is clear that this is a modest starburst.

(xi) *ISOHDFS J223252-603327.* This radio source, detected solidly at 1.4 GHz, is at the centre of extended emission in both *ISO* bands, which may explain why the mid-infrared fluxes slightly exceed the predictions of the starburst models. The radio detection is in excellent agreement with the Arp 220 model, and if we adopt that we obtain $500\,{\rm M}_{\odot}\,{\rm yr}^{-1}$, using the integrated $L_{\rm IR}$ estimator. It was noted in Section 2.3 that this source becomes more point-like at longer wavelengths, as one passes through the optical into the near-infrared, so it could contain an obscured AGN, and hence the SFR estimated here may be an over-estimate.

(xii) *ISOHDFS J223254-603115.* As noted in Section 2.3, there appears to be a mismatch in the apertures used for the optical and near-infrared photometry of this galaxy. If we normalize the GRASIL models to the *K*-band magnitude of this galaxy, then we see that its SED is in good agreement with the NGC 6090 and M82 models, with the Arp 220 model marginally disfavoured by the lack of a radio detection. Applying the integrated $L_{\rm IR}$ estimator to the NGC 6090 model we obtain an SFR of $11\,{\rm M}_{\odot}\,{\rm yr}^{-1}$, which we adopt as our best guess; if, instead, the M82 model were used, that figure would be negligibly higher, at $12\,{\rm M}_{\odot}\,{\rm yr}^{-1}$.

(xiii) *ISOHDFS J223254-603129.* From Fig. 6 we see that the *ISO* fluxes of this source are in good agreement with the three starburst model SEDs, when they are normalized using the *K*-band magnitude of the galaxy. If we apply the integrated $L_{\rm IR}$ estimator to the NGC 6090 model, which gives the best overall fit, we obtain a best-guess SFR estimate of $1.2\,{\rm M}_{\odot}\,{\rm yr}^{-1}$.

(xiv) *ISOHDFS J223257-603305.* The 15-μm to near-infrared colour of this galaxy implies that it is a starburst, and the lack of radio detections excludes a burst as extreme as Arp 220. Taking the NGC 6090 model, we obtain an SFR estimate of $43\,{\rm M}_{\odot}\,{\rm yr}^{-1}$, using the integrated $L_{\rm IR}$ estimator, and we adopt this as our best guess.

(xv) *ISOHDFS J223302-603323.* Fig. 6 shows that this source is securely identified as a cirrus galaxy, rather than a starburst, and, adopting the M100 model, we obtain a best-guess SFR of $10\,{\rm M}_{\odot}\,{\rm yr}^{-1}$, using the integrated $L_{\rm IR}$ estimator.

(xvi) *ISOHDFS J223303-603336.* The 7-μm to near-infrared colour of this source suggests that it is a starburst, rather than a cirrus galaxy, but the lack of a 15-μm detection is puzzling, in that case, although once again it may be due to uncertainty in the subtraction of the negative lobes from a nearby source that is bright in both *ISO* bands. The Arp 220 SED is ruled out by the lack of radio detections, and, if we adopt the NGC 6090 model, we obtain

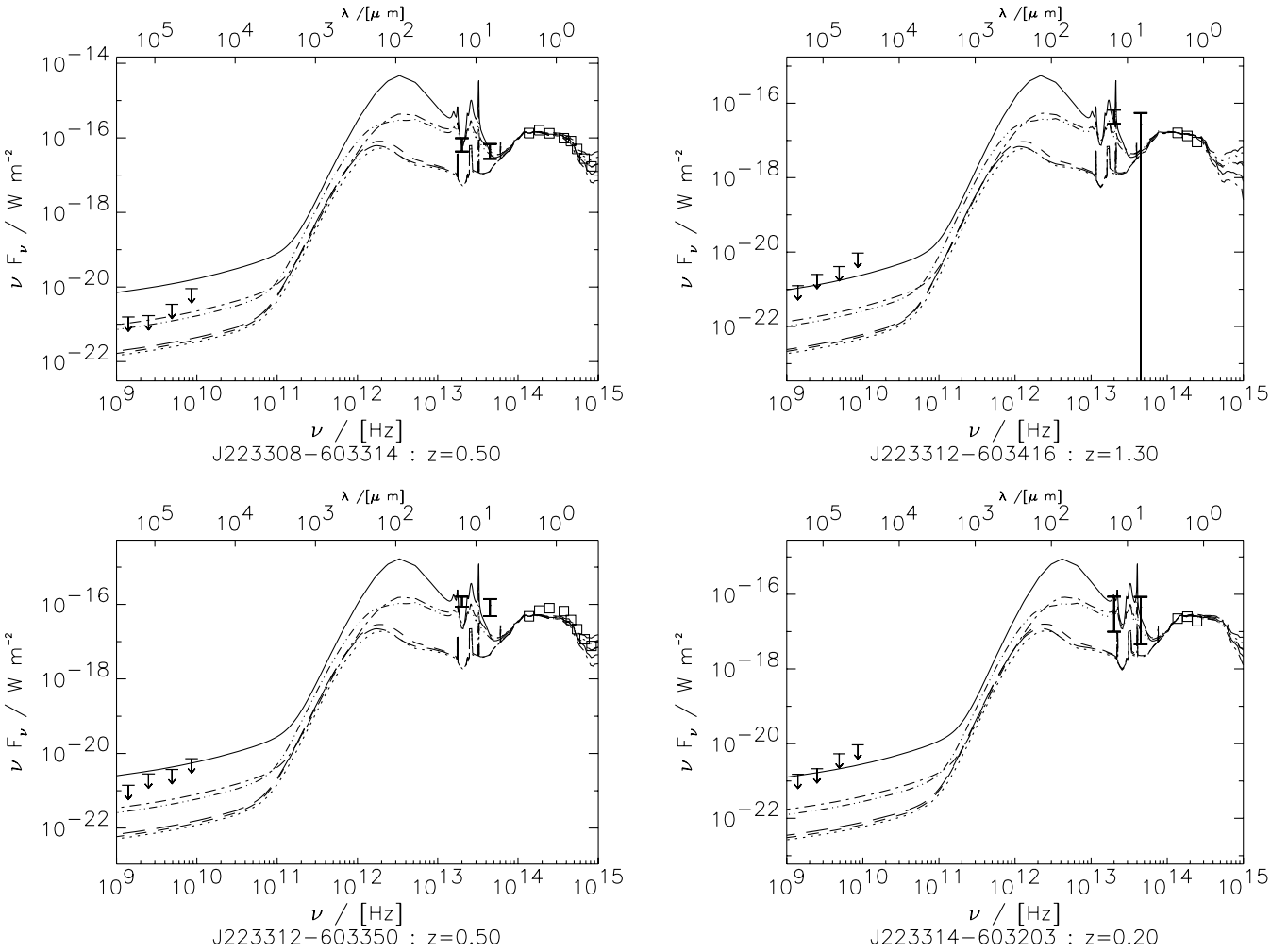

Figure 6 – *continued*

an SFR of $16\,M_\odot\,yr^{-1}$ using the integrated L_{IR} estimator, while, if the M100 model is preferred, this falls to $2\,M_\odot\,yr^{-1}$. We shall adopt a best guess of $5\,M_\odot\,yr^{-1}$, but note that this is one of our most uncertain SFR estimates.

(xvii) *ISOHDFS J223306-603349.* From Fig. 6 we see that this galaxy was detected in the radio at 1.4 and 2.5 GHz at almost exactly the level expected for the GRASIL NGC 6090 SED normalized to the observed *K*-band magnitude of the galaxy, but that the two *ISO* fluxes look a little low to match that interpretation, especially the 15-μm flux. The radio detections are a strong indication that this is a starburst rather than a cirrus galaxy, however, so we do adopt the NGC 6090 SED which yields a best-guess SFR of 60-$M_\odot\,yr^{-1}$ from the integrated L_{IR} estimator, although we record that, if we had adopted an NGC 6946 SED, this would have fallen to $10\,M_\odot\,yr^{-1}$.

(xviii) *ISOHDFS J223306-603436.* The mid-infrared colour of this source suggests that it is a starburst, rather than a cirrus galaxy, and its optical/near-infrared colours fit an (appropriately normalized) M82 model all the way from the *B* to the *K*-band. Adopting that SED yields a best-guess SFR of $74 \pm 15\,M_\odot\,yr^{-1}$.

(xix) *ISOHDFS J223306-603450.* As illustrated in Fig. 6, the 15-μm/near-infrared colour of this source is that of a starburst, not a cirrus galaxy, but the extant data are not able to distinguish between an Arp 220-type galaxy and a more modest burst, like M82, with the lack of detections at 7 μm and in the radio consistent with both possibilities. The Arp 220 SED would yield an SFR of $130\,M_\odot\,yr^{-1}$, while the M82 model gives $17\,M_\odot\,yr^{-1}$, so we shall adopt an admittedly uncertain compromise figure of $50\,M_\odot\,yr^{-1}$ as our best-guess SFR.

(xx) *ISOHDFS J223307-603248.* We cannot unambiguously distinguish whether this source is a starburst or cirrus galaxy. The 7-μm/15-μm colours favour the former, as does the shape of its ultraviolet/optical/near-infrared SED, and if we adopt the NGC 6090 SED we obtain an SFR estimate of $65\,M_\odot\,yr^{-1}$, while a lower value of $10\,M_\odot\,yr^{-1}$ would result from using an M100 model instead. We shall adopt the former value as our best guess, but note that we cannot confidently exclude an SFR value a factor of 4 lower.

(xxi) *ISOHDFS J223308-603314.* This source is solidly identified as a starburst, as its SED fits the GRASIL NGC 6090 model from the *U* band all the way to 15 μm. With that SED we estimate its SFR to be $46\,M_\odot\,yr^{-1}$, using the integrated L_{IR} estimator.

(xxii) *ISOHDFS J223312-603350.* As noted in Section 2.3, the redshift of this galaxy is highly uncertain, and hence so is its SFR. The shape of its ultraviolet/optical/near-infrared SED suggests that it is a starburst, as, more strongly, does its mid/near-infrared colour, but it is difficult to judge the strength of its burst from the extant

data. We adopt an NGC 6090 SED to obtain a best-guess SFR estimate of $15\,M_\odot\,yr^{-1}$, although we note that choosing an Arp 220 model instead would have yielded $130\,M_\odot\,yr^{-1}$.

(xxiii) *ISOHDFS J223312-603416.* This is another source with a very uncertain redshift, based only on *JHK* photometry, and furthermore its 7-μm flux is highly uncertain, owing to its being located in a region of extended 7-μm emission, as shown in Fig. 4. The 15-μm/near-infrared colour of this source suggests that it is a starburst, and the Arp 220 and NGC 6090 SEDs give SFR estimates of 370 and $46\,M_\odot\,yr^{-1}$, respectively. We adopt a value of $100\,M_\odot\,yr^{-1}$ as our best guess, but noting that, in addition to the uncertainty caused by the poorly constrained SED, there is also uncertainty over the redshift of this galaxy.

(xxiv) *ISOHDFS J223314-603203.* Another source with a mid/near-infrared colour that indicates it to be a starburst, rather than a cirrus galaxy, but for which we are unable to assess the strength of the burst given the current data. The Arp 220 and NGC 6090 SED models give SFR estimates of 9 and $1\,M_\odot\,yr^{-1}$, respectively, indicating either way that this is a modest starburst; we shall adopt a value of $3\,M_\odot\,yr^{-1}$ as our best guess, noting that Section 3 showed this to be one of our most uncertain associations.

5 THE CONTRIBUTION OF *ISO*-SELECTED SOURCES TO THE STAR FORMATION HISTORY OF THE HDF-S

In Fig. 7 we plot the distribution of SFR values for 22 *ISO* HDF-S sources that we believe to be star-forming galaxies, omitting the galaxy with the highest SFR (ISOHDFS J223252-603327 at $500\,M_\odot\,yr^{-1}$), which may be harbouring an obscured AGN. As can be seen from this, the *ISO* HDF-S galaxies are typically active starbursts (median SFR $= 43\,M_\odot\,yr^{-1}$), although they do cover a range of two orders of magnitude in SFR. These values are computed under the assumption of an Einstein–de Sitter universe with a Hubble constant of $H_0 = 50\,km\,s^{-1}\,Mpc^{-1}$. Using the slightly non-linear integrated L_{IR} estimator of Devriendt et al. (1999), we have the SFR varying with luminosity distance, d_L, as $d_L^{2.1}$, and hence with Hubble constant as $H_0^{0.48}$. If, instead, we had assumed a cosmology with $\Omega_M = 0.7$ and $\Omega_\Lambda = 0.3$, we would have deduced, for the same value of H_0, SFR values that were factors of 11, 20, 47 and 78 per cent higher for galaxies at redshifts of 0.1, 0.2, 0.5 and 1.0 respectively.

For five of our galaxies, SFR estimates have been made by Rigopoulou et al. (2001), on the basis of Hα luminosity and also using a far-infrared estimator (Franceschini et al., in preparation) which makes use of the 15-μm flux and assumes a far-infrared/mid-infrared luminosity ratio of ~ 10 as appropriate for a galaxy with a spectral energy distribution like that of M82. Rigopoulou et al. (2001) assumed a cosmology with $\Omega_M = 0.7$ and $\Omega_\Lambda = 0.3$ and a Salpeter (1955) IMF over the mass range $[1,100]\,M_\odot$, so, before we can compare their results with ours, we must scale their SFR values to account for these effects, using methods discussed in Appendix A. Under our canonical assumptions, their far-infrared-based estimator gives SFR values of 113, 89, 69, 220 and $65\,M_\odot\,yr^{-1}$ for galaxies J223245-603418, J223245-603226, J223247-603335, J223252-603327 and J223257-603305, respectively, for which our adopted values are 100, 36, 50, 500 and $43\,M_\odot\,yr^{-1}$, which is a reasonable level of agreement, given the uncertainties in the true SEDs of these sources. With the appropriate scalings, the Hα-based estimator of Rigopoulou et al. (2001) gives SFR raw values of 2.1, 6.0, 5.9, 74 and $12\,M_\odot\,yr^{-1}$ for these five galaxies, which are factors of 5–50 smaller than those estimated from the far-infrared. Rigopoulou et al. (2001) argue that, on the basis of the $V - K$ colours of these galaxies, one would deduce an extinction correction of only ~ 4 to the Hα SFR, suggesting that optical data alone are not sufficient to derive a good SFR value, even when they do yield an extinction correction; this is in accordance with the work of Silva et al. (1998) and Jimenez et al. (1999), mentioned previously, who argue on theoretical grounds that the emission from star-forming regions cannot be well represented by a simple model of a dust-screen in front of a dust-free starburst.

5.1 Computing the raw star formation rate density

We may use these SFR estimates to derive constraints on the star formation history of the Universe, at least in the redshift interval in which our sources are found, i.e. $z \leq 0.6$ for the most part. In fact, as Fig. 8 shows, the redshift distribution of the galaxies associated

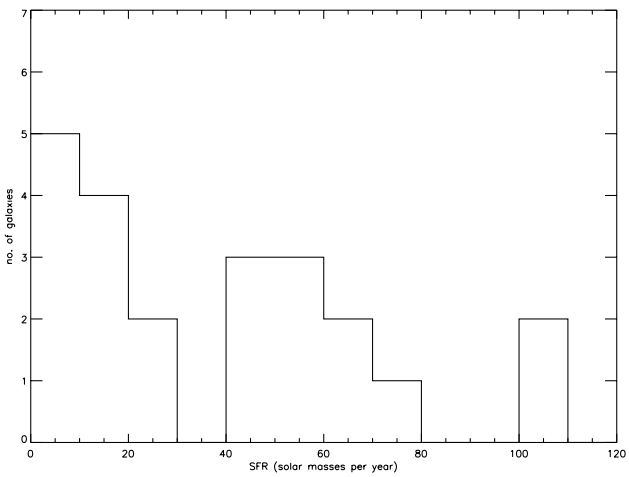

Figure 7. The distribution of SFRs for the 22 *ISO* HDF-S sources that we believe to be star-forming galaxies, omitting the galaxy with the highest SFR (ISOHDFS J223252-603327 at $500\,M_\odot\,yr^{-1}$), which may be harbouring an obscured AGN.

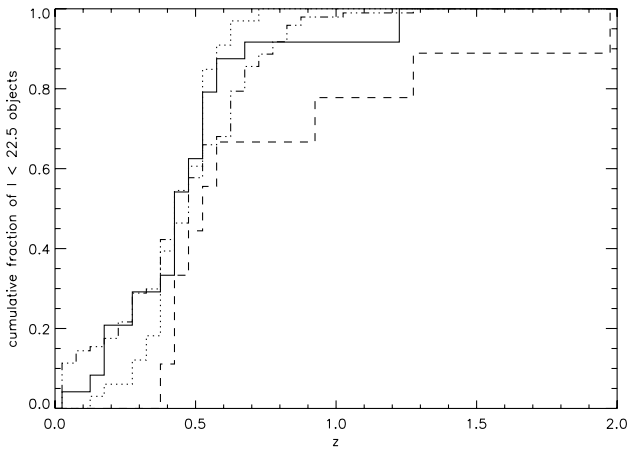

Figure 8. A comparison of the cumulative redshift distributions of the *ISO* HDF-S galaxy sample (solid line) with those from three HDF-S photometric redshift catalogues: the double-dot–dashed line is that of MRR, the dashed line that of Gwyn (1999), and the dotted line that of the SUNY group.

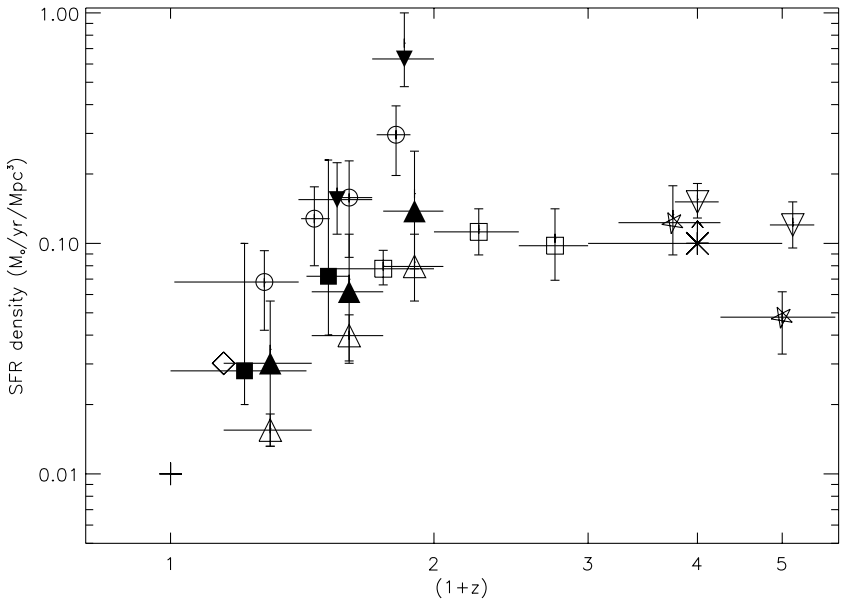

Figure 9. A compilation of constraints on the star formation history of the Universe, mainly taken from Haarsma et al. (2000): in all cases, an Einstein–de Sitter universe, with a Hubble constant of $50\,\mathrm{km\,s^{-1}\,Mpc^{-1}}$ was assumed, as was star formation taking place with a Salpeter (1955) IMF, over the mass range [0.1, 100] $\mathrm{M_\odot}$, and the dust extinction corrections of Steidel et al. (1999) were applied. The symbols are as follows: asterisk – Hughes et al. (1998); filled upward-pointing triangle – Flores et al. (1999); empty square – Connolly et al. (1997); plus sign – Gallego et al. (1995); empty downward-pointing triangle – Steidel et al. (1999); five-pointed star – Madau et al. (1996); diamond – Treyer et al. (1998); filled downward-pointing triangle – Rowan-Robinson et al. (1997); empty upward-pointing triangle – Lilly et al. (1996); empty circle – Haarsma et al. (2000); filled square – this work, with confidence intervals computed according to the sampling variance treatment of Appendix B, assuming $\sigma^2 = 1$.

with our *ISO* sources is consistent with that of similarly bright (i.e. $I < 22.5$) galaxies in the HDF-S as a whole, at least as judged from photometric redshift catalogues produced for the field: two-sided Kolmogorov–Smirnov tests reveal that the cumulative redshift distribution of the *ISO* identifications has probabilities of 0.30, 0.43 and 0.75 of being drawn from the same population as that yielding the $n(z)$ distributions found in the photometric redshift catalogues of MRR, Gwyn (1999) and the SUNY group, respectively.

We divide this region into two equal volume bins ($0 \leq z < 0.43$ and $0.43 \leq z \leq 0.6$), in which we compute the SFR density, via the available volume technique. The volume in which each galaxy could have been observed within any given redshift slice was estimated by considering its luminosity and best-fitting SED and hence determining the effective area over which it could have been observed at given redshift using the area as a function of 15-μm flux limits (fig. 13 of Paper I). The contribution of each galaxy to the global SFR density, $\dot{\rho}_*$, was then calculated as the ratio between the SFR determined for that galaxy and its available volume, and the sum of these individual contributions was then taken over all galaxies in each bin. Note that there exists one galaxy (ISOHDF J223303-603336, which may be affected by the lobe subtraction problem) lying in the range $z < 0.6$ which does not have a detection at 15-μm. Whether this galaxy is excluded, or included, using an available volume computed with an estimate of what its 15-μm flux 'should' be, on the basis of the best-fitting GRASIL SED, makes a negligible difference to the raw value of $\dot{\rho}_*$ obtained, so for definiteness we neglect it, leaving us with a 15-μm-selected sample.

This yields values of $\dot{\rho}_* = 0.03 \pm 0.2\,\mathrm{dex}$ (i.e. $\dot{\rho}_* = 0.03^{+0.02}_{-0.01}$) and $\dot{\rho}_* = 0.07 \pm 0.1\,\mathrm{dex}$ (i.e. $\dot{\rho}_* = 0.07^{+0.02}_{-0.01}$) $\mathrm{M_\odot\,yr^{-1}\,Mpc^{-1}}$ for $0 \leq z \leq 0.43$ and $0.43 \leq z \leq 0.6$, respectively, where we have assumed an Einstein–de Sitter universe, and star formation according to a Salpeter (1955) IMF over the mass range [0.1, 100] $\mathrm{M_\odot}$ and taken our SFR estimates for individual galaxies to be uncertain by a factor of 2. In Fig. 9 we show a comparison of these results and a compilation (principally that of Haarsma et al. 2000) of similar constraints derived recently from a variety of methods in a number of wavebands, all using the same assumed cosmology and IMF. One notable feature of this is that our raw results are in excellent agreement with another recent study using *ISO* data, that of Flores et al. (1999) based on their study of the CFRS 1415+52 field.

5.2 Sampling variance in our $\dot{\rho}_*$ results

The relatively small volume of our survey region means that our SFR density values are subject to a relatively large sampling variance. The volume of a cone $0 < z < 0.43$ with solid angle 20 arcmin^2 (equal to our survey area) is $\sim 520\,h^{-3}\,\mathrm{Mpc^3}$, while a frustum with the same solid angle and $0.43 \leq z \leq 0.6$ is $\sim 570\,h^{-3}\,\mathrm{Mpc^3}$. We can thus consider each survey section to have a volume of $\sim 550\,h^{-3}\,\mathrm{Mpc^3}$; cubic cells of the same volume would have sides of $8.2\,h^{-1}\,\mathrm{Mpc}$, while spheres would have radii of $5.0\,h^{-1}\,\mathrm{Mpc}$. These volumes are small enough that the variations in mean density between surveys carried out in different regions of the Universe are expected to be significant. Using the power spectrum of Peacock & Dodds (1994) and the conversion from length-scale to effective wavenumber for cubic cells (Peacock 1991), we estimate that the fractional density fluctuations in cubic cells of this volume at redshift zero will be $\sigma^2 = 1.05$, while that of spheres would have $\sigma^2 = 1.15$. Note that the variances in local cells with the same geometry as our survey volumes are likely to be larger than this, as their elongated shape would lead to a window function that lets in more small-scale power than spherical or cubic window functions do. Several more effects further complicate an assessment of the sampling variance in our SFR density estimates.

First, there is evolution in the density field with redshift across the two sampling volumes. At $z = 0.2$ and 0.5, in the middle of our two redshift bins, the linear theory variances in a given volume would be factors of $(1+z)^2$, i.e. 1.4 and 2.3, respectively, below their values at redshift zero, while non-linear effects as $\sigma \rightarrow 1$ are likely to make the decrease more pronounced than these linear theory estimates suggest. Furthermore, the shape of our survey volumes means that they have more volume at higher redshift, where the density field is less evolved. A further complicating factor is the bias between the galaxy and mass distributions, which is likely to lead to a higher sampling variance for the total SFRs in our two redshift bins than that for the mass they contain, and an additional uncertainty in the redshift variation across the bins: Kauffmann et al. (1999) show that the evolution of galaxy clustering strength over $0 \leq z \leq 1$ is a function of cosmology, at least in their galaxy formation models. Clearly, the quantitative assessment of these various factors is beyond the scope of the current paper, so we shall base this study of the effects of sampling variance on $\dot{\rho}_*$ estimates on the assumption that the variance in the mass contained in our two redshift bins is $\sigma^2 \sim 1$ and that $\sigma^2 = 0.5$ and 2 are likely to be conservative bounds to the true values.

The variance σ^2 is equal to $\sigma_\rho^2/\bar{\rho}^2$, where σ_ρ^2 is the variance in the mass density field, and $\bar{\rho}$ is its mean value. A crude approach would be then to argue that

$$\sigma = \frac{\sigma_\rho}{\bar{\rho}} \sim \frac{\sigma_\rho}{\rho} = \sigma_{\ln \rho}, \tag{10}$$

in which case $\sigma_{\log_{10}\rho} = \log_{10}(\mathrm{e})\sigma$. This would then mean that the estimates for $\dot{\rho}_*$ in our lower (higher) redshift bins would have sampling errors of ± 0.52 dex (± 0.34 dex), respectively, so that the sampling variance in $\dot{\rho}_*$ exceeds the uncertainty from the individual SFR estimates for both bins.

This method neglects the fact that, since $\sigma^2 \sim 1$, the probability distribution function (PDF) for the cosmological density field will have been significantly skewed by gravitational evolution. This skewness will be reflected in strongly asymmetric error bars on our $\dot{\rho}_*$ estimates owing to sampling variance; with such a skewed PDF, our randomly selected survey volume (the selection of the HDF-S region was based on the presence of a $z \sim 2$ quasar, which should have no bearing on the properties of galaxies at $z \leq 1$) is much more likely to be underdense than overdense, and hence we are much more likely to have measured a value of $\dot{\rho}_*$ that is lower than the global mean than one higher than it. Estimating the level of such an effect is very difficult. A full analysis would require a large numerical simulation of the cosmological density field, coupled to a galaxy formation model capable of predicting accurately the sites of formation of the class of galaxies detected in our *ISO* survey, which is far beyond the scope of this paper. Simple analytic model prescriptions do exist for following the gravitational evolution of the PDF, but most are based on approximations (e.g. perturbation theory or the Zel'dovich approximation) that break down by $\sigma \sim 1$. Bernardeau & Kofman (1995) have, however, shown that a lognormal model continues to give a good fit to the PDF derived from *N*-body simulations of a cold dark matter universe until at least $\sigma \sim 1.5$, so this is one analytic form that might be used.

In Appendix B we show how this approximation may be used, within a Bayesian framework, to compute the 68 per cent confidence intervals for $\bar{\rho}_*$, the *global* SFR density at the redshifts corresponding to the centres of our two bins, given our raw $\dot{\rho}_*$ values and our estimate that the matter variance in cells of size equal to our survey volumes is $0.5 \leq \sigma^2 \leq 2$. This analysis reveals that, for a best guess of $\sigma^2 = 1$, $0.62 \leq \bar{\rho}_*/\hat{\rho}_* \leq 3.2$, while increasing or decreasing σ^2 by a factor of 2 barely changes the lower limit to $\bar{\rho}_*/\hat{\rho}_*$, while the upper limit increases to 5.0 or decreases to 2.3, respectively. Thus we see that sampling variance introduces a larger uncertainty into the estimation of $\dot{\rho}_*$ than that caused by the uncertainties in the SFRs of the individual galaxies in our survey. Assuming $\sigma^2 = 1$, we estimate $0.02 \leq \bar{\rho}_* \leq 0.10$ and $0.04 \leq \bar{\rho}_* \leq 0.23\,\mathrm{M}_\odot\,\mathrm{yr}^{-1}\,\mathrm{Mpc}^{-3}$ for the $z < 0.43$ and $0.43 \leq z \leq 0.6$ bins, respectively, where we define confidence intervals solely using our sampling variance analysis.

We plot these confidence intervals in Fig. 9. These results are model-dependent, and neither the simple variance estimation nor the lognormal model of Appendix B is satisfactory, but both indicate that there is a large uncertainty associated with $\dot{\rho}_*$ estimates determined from volumes as small as our *ISO* survey of the HDF-S. Our results are consistent with the *ISO* -based results of Flores et al. (1999) (whose CFRS field is an order of magnitude larger, and so should yield $\dot{\rho}_*$ values with much lower sampling variances) and with the radio-based results of Haarsma et al. (2000), but it is clear that, given the large sampling variance inevitable for such a small survey volume, they cannot place tight constraints on the star formation history of the Universe by themselves.

6 DISCUSSION AND CONCLUSIONS

In this paper and its companion (Paper I) we have presented results from our *ISO* survey of the *Hubble Deep Field* South. Here we sought optical identifications for the *ISO* sources found in Paper I, obtaining reliable associations for 32 out of the 35 sources: these associations should be more secure than those made by Mann et al. (1997) using our initial analysis of our corresponding *ISO* survey of the northern *Hubble Deep Field*, thanks to the inclusion of corrections for ISOCAM image distortions, which were not well characterized in 1997. Of these 32 sources, a total of 22 were identified as spiral or starburst galaxies, eight of which have spectroscopic redshifts [from the work of Rigopoulou et al. (2001) and Glazebrook et al. (in preparation)] and the remaining 14 of which have had photometric redshifts estimated by ourselves and others. We estimate that our photometric redshifts should be accurate to $\delta z = 0.1$ or so, on the basis of the set of eight objects for which spectroscopic redshifts are known, although we have noted individual cases where the error is likely to be greater than that, for example when a redshift has been estimated solely on the basis of *JHK* photometry. We find that the redshift distribution of the galaxies associated with our *ISO* sources is consistent with that for similarly bright optical galaxies in the HDF-S region as a whole.

We have reviewed a series of methods commonly used to determine SFRs for galaxies in survey data, typically comprising a single broad-band flux for each object. We have assessed the ability of these to reproduce the SFRs of models of actively star-forming galaxies, finding, as others (e.g. Granato et al. 2000) have, that those probing their far-infrared emission fared much better than those based on ultraviolet luminosity, indicating that massive star formation in these galaxies takes place in dusty regions: the work of Rigopoulou et al. (2001) shows further that this dust obscuration is not well corrected for using optically determined extinction values. All these methods look for indications of the formation of massive stars, so a further complication in the determination of the absolute rate at which stellar mass is being formed in a given galaxy is uncertainty in the IMF, since the vast majority of the mass resides in stars not directly probed by these methods, so SFR estimates differing by factors of a few can result if differing IMFs

are assumed. Caution must be exercised when applying these estimators in situations where the SED types of the galaxies under study are constrained only by a small number of broad-band fluxes, suggesting that constraints on the cosmic star formation history are best obtained in well-studied fields, such as the *Hubble Deep Fields*, where rich, multiwavelength data sets are available. The small areas of the *Hubble Deep Fields* do, however, mean that significant sampling variances exist for estimates of $\dot{\rho}_*$ at $z \leq 1$, and we have shown, via two simple methods for assessing their magnitude, that while our results are consistent with those of previous authors, notably Flores et al. (1999) and Haarsma et al. (2000), they cannot by themselves yield tight constraints on the star formation history of the Universe, owing to these sampling effects. Further details of this project can be found at http://astro.ic.ac.uk/hdfs.

ACKNOWLEDGMENTS

This paper is based on observations with *ISO*, an ESA project, with instruments funded by ESA Member States (especially the PI countries: France, Germany, the Netherlands and the United Kingdom) and with participation of ISAS and NASA. This work was in part supported by PPARC grant No. GR/K98728 and EC Network is FMRX-CT96-0068. We thank the ATNF HDF-S team, particularly Andrew Hopkins, for providing us with radio data for our sources in advance of publication, and an anonymous referee for comments.

REFERENCES

Acosta-Pulido J. A. et al., 1996, A&A, 315, L121
Bernardeau F., Kofman L., 1995, ApJ, 443, 479
Bertin E., Arnouts S., 1996, A&A, 117, 393
Binney J., Merrifield M., 1998, Galactic Astronomy. Princeton Univ. Press, Princeton, NJ
Cesarsky C. J. et al., 1996, A&A, 315, L32
Condon J. J., 1992, ARA&A, 30, 575
Connolly A. J., Szalay A. S., Dickinson M., SubbaRao M. U., Brunner R. J., 1997, ApJ, 486, L11
Cram L., Hopkins A., Mobasher B., Rowan-Robinson M., 1998, ApJ, 507, 155
da Costa L. et al., 1998, astro-ph/9812105
Devriendt J. E. G., Guiderdoni B., Sadat R., 1999, A&A, 350, 381
Efstathiou A., Rowan-Robinson M., Siebenmorgen R., 2000, MNRAS, 313, 734
Fioc M., Rocca-Volmerange B., 1997, A&A, 326, 950
Flores H. et al., 1999, ApJ, 517, 148
Gallego J., Zamorano J., Aragon-Salamanca A., Rego M., 1995, ApJ, 455, L1
Gardner J. P. et al., 1999, http://hires.gsfc.nasa.gov/~gardner/hdfs/
Genzel R. et al., 1998, ApJ, 498, 579
Goldschmidt P. et al., 1997, MNRAS, 289, 465
Granato G. L., Lacey C. G., Silva L., Bressan A., Baugh C. M., Cole S., Frenk C. S., 2000, ApJ, 542, 710
Gwyn S., 1999, http://astrowww.phys.uvic.ca/grads/gwyn/pz/hdfs/spindex.html
Haarsma D. B., Partridge R. B., Windhorst R. A., Richards E., 2000, ApJ, 544, 641
Hughes D. et al., 1998, Nat, 394, 241
Jimenez R., Friaca A. C. S., Dunlop J. S., Terlevich R. J., Peacock J. A., Nolan L. A., 1999, MNRAS, 305, L16
Kauffmann G., Colberg J. M., Diaferio A., White S. D. M., 1999, MNRAS, 307, 529
Kennicutt R. C., 1998, ARA&A, 36, 189
Kessler M. F. et al., 1996, A&A, 315, L27
Lilly S. J., LeFèvre O., Crampton D., Hammer F., Tresse L., 1995, ApJ, 455, 50
Lilly S. J., LeFèvre O., Hammer F., Crampton D., 1996, ApJ, 460, L1
Madau P., Ferguson H. C., Dickinson M. E., Giavalisco M., Steidel C. C., Fruchter A., 1996, MNRAS, 283, 1388
Mann R. G. et al., 1997, MNRAS, 289, 482
Miller G. E., Scalo J. M., 1979, ApJS, 41, 513
Oliver S. J. et al., 1997, MNRAS, 289, 471
Oliver S. J. et al., 2002, MNRAS, 332, 536 (Paper I, this issue)
Peacock J. A., 1991, MNRAS, 253, 1P
Peacock J. A., Dodds S. J., 1994, MNRAS, 267, 1020
Persson S. E., Murphy D. C., Krzeminski W., Roth M., Rieke M. J., 1998, AJ, 116, 2475
Rigopoulou D. et al., 2001, ApJ, 537, L85
Rowan-Robinson M., 2001, ApJ, submitted
Rowan-Robinson M., Crawford J., 1989, MNRAS, 238, 523
Rowan-Robinson M. et al., 1997, MNRAS, 289, 490
Rutledge R. E., Brunner R. J., Prince T. A., Lonsdale C., 2000, ApJS, 131, 335
Salpeter E. E., 1955, ApJ, 121, 161
Serjeant S. B. G. et al., 1997, MNRAS, 289, 457
Silva L., 1999, PhD thesis, SISSA
Silva L., Granato G. L., Bressan A., Danese L., 1998, ApJ, 509, 103
Steidel C. C., Adelberger K. L., Gavalisco M., Dickinson M., Pettini M., 1999, ApJ, 519, 1
Sutherland W., Saunders W., 1992, MNRAS, 259, 413
Telesco C. M., Gatley I., 1984, ApJ, 284, 557
Thronson H. A., Telesco C. M., 1986, ApJ, 311, 98
Treyer M. A., Ellis R. S., Milliard B., Donas J., Bridges T. J., 1998, MNRAS, 300, 303
Walker A., 1999, http://icarus.stsci.edu/~ferguson/hdfstest/hdfs_astro.fits
Williams R. E. et al., 1996, AJ, 112, 1335
Yoshii Y., Takahara F., 1988, ApJ, 326, 1

APPENDIX A: CONVERSION OF STAR FORMATION RATE ESTIMATORS TO A CANONICAL INITIAL MASS FUNCTION

As mentioned in Section 3.2, there are three types of physical model underlying the SFR estimators of equations (2)–(8). It follows, by the definition of $\dot{M}$, the rate of formation of stellar mass (in $\mathrm{M}_\odot\,\mathrm{yr}^{-1}$), that

$$\dot{M} = \int_{M_\mathrm{L}}^{M_\mathrm{U}} M\psi(M)\,\mathrm{d}M, \tag{A1}$$

where $\psi(M)$ is the IMF, and stars are being formed over the mass range $[M_\mathrm{L}, M_\mathrm{U}]$.

The first class are those [from equations (5), (6) and (7)] based on the assumption (Thronson & Telesco 1986; Rowan-Robinson et al. 1997) that some large ($\epsilon \simeq 1$) fraction of the bolometric luminosity, L_bol, generated in any burst of star formation emerges in the far-infrared, owing to the reprocessing by dust of the light from young stars: i.e.

$$L_\mathrm{FIR} = \epsilon L_\mathrm{bol} = \epsilon \int_{M_\mathrm{L}}^{M_\mathrm{U}} L(M) t_\mathrm{FIR}(M) \psi(M)\,\mathrm{d}M, \tag{A2}$$

where $L(M)$ is the luminosity of a newly formed star of mass M (and it is assumed that only main-sequence stars contribute) and that such stars contribute to L_FIR for time $t_\mathrm{FIR}(M)$. The crucial time-scale here is the time taken for the dust cloud around the young star to be destroyed and that is assumed (Thronson & Telesco 1986) to be independent of mass, and to be $\tau_\mathrm{FIR} \sim O(10^6\,\mathrm{yr})$, in which case

$$L_\mathrm{FIR} = \epsilon \tau_\mathrm{FIR} \int_{M_\mathrm{L}}^{M_\mathrm{U}} L(M)\psi(M)\,\mathrm{d}M, \tag{A3}$$

so that, combining equations (A1) and (A3),

$$\dot{M} \propto L_{\rm FIR} \frac{\int_{M_{\rm L}}^{M_{\rm U}} M\psi(M)\,{\rm d}M}{\int_{M_{\rm L}}^{M_{\rm U}} L(M)\psi(M)\,{\rm d}M} \propto L_{\rm FIR}\frac{\bar{M}}{\bar{L}_{\rm bol}}, \tag{A4}$$

where $\bar{M}$ and $\bar{L}_{\rm bol}$ are, respectively, the average mass and bolometric luminosity of stars formed according to the particular IMF: i.e.

$$\bar{M} = \frac{\int_{M_{\rm L}}^{M_{\rm U}} M\psi(M)\,{\rm d}M}{\int_{M_{\rm L}}^{M_{\rm U}} \psi(M)\,{\rm d}M} \tag{A5}$$

and

$$\bar{L} = \frac{\int_{M_{\rm L}}^{M_{\rm U}} L(M)\psi(M)\,{\rm d}M}{\int_{M_{\rm L}}^{M_{\rm U}} \psi(M)\,{\rm d}M}. \tag{A6}$$

So we have shown, following Thronson & Telesco (1986), that the SFR (in $\mathrm{M_\odot\,yr^{-1}}$) per unit of far-infrared luminosity (say, at 60 μm, or integrated over 3–1000 μm) is proportional to $\bar{M}/\bar{L}_{\rm bol}$.

Several choices exist for the form of $L(M)$ to use. Telesco & Gatley (1984) assume a double-power-law form, namely $L(M)/{\rm L_\odot} = A(M/{\rm M_\odot})^\alpha$, where

$$(A,\alpha) = \begin{cases} (1.3, 3.6): & 0.1 \le M/{\rm M_\odot} \le 10, \\ (8.1, 2.8): & 10 \le M/{\rm M_\odot} \le 60, \end{cases} \tag{A7}$$

using which yields the following set of $\bar{M}/\bar{L}_{\rm bol}$ values for the $\psi(M) \propto M^{-x}$ models of interest here:

$$\frac{\bar{M}/\bar{L}_{\rm bol}}{10^{-3}\,\bar{\rm M}_\odot/\bar{\rm L}_\odot} = \begin{cases} 1.33 : (M_{\rm L}, M_{\rm U}) = (0.1, 100)\,{\rm M_\odot}, x = 2.35, \\ 1.02 : (M_{\rm L}, M_{\rm U}) = (0.1, 120)\,{\rm M_\odot}, x = 2.35, \\ 2.52 : (M_{\rm L}, M_{\rm U}) = (0.1, 100)\,{\rm M_\odot}, x = 2.50, \end{cases} \tag{A8}$$

reproducing the results in table 3 of Thronson & Telesco (1986), from which Rowan-Robinson et al. (1997) derived the value that ϕ should take in equation (5) for different choices of IMF. Following this method, we find that to match our reference IMF requires having $\phi = 1$ in equation (5), and multiplying the SFR deduced from equation (7) by a factor of $(1.33/1.02)^{1.05} = 1.32$ to account for the fact that Devriendt et al. (1999) use a Salpeter IMF with an upper mass limit of $120\,{\rm M_\odot}$.

To calculate the scaling appropriate for the 60-μm estimator of Cram et al. (1998), we must account for not only the different $\bar{M}/\bar{L}_{\rm bol}$ values for their IMF and our reference Salpeter (1955) law (given above), but also the fact that they quote an SFR which refers to stars of mass $M \ge 5\,{\rm M_\odot}$, which is done as follows. Only one-ninth of the stellar mass formed with their IMF is in stars of $M \ge 5\,{\rm M_\odot}$, with the result that the SFR value from equation (6) must be multiplied by a factor of $9/(2.52/1.33) = 4.8$ to make it appropriate for the formation of stars according to our reference IMF.

The second class of methods comprises the three SFR estimators based on monochromatic ultraviolet luminosities. In this case, the factors of $\bar{M}/\bar{L}_{\rm bol}$ in the scaling are replaced by $\bar{M}/\bar{L}_\lambda$, where $\bar{L}_\lambda$ is the mean value of the particular monochromatic luminosity under consideration, evaluated over the stars formed according to the given IMF. Values for $\bar{L}_\lambda$ can be readily computed under the assumption that main-sequence stars emit as blackbodies in the ultraviolet. This we implement, making double- and triple-power–law fits, respectively, to the main-sequence radius–mass and effective temperature–mass relation data tabulated by Binney & Merrifield (1998), i.e.

$$\log_{10}\left(\frac{R}{\rm R_\odot}\right) = \begin{cases} 0.02 + 0.72\log_{10}(M/{\rm M_\odot}): & M/{\rm M_\odot} \le 10, \\ 0.30 + 0.44\log_{10}(M/{\rm M_\odot}): & M/{\rm M_\odot} \ge 10, \end{cases} \tag{A9}$$

and

$$\log_{10}\left(\frac{T_{\rm eff}}{10^3\,{\rm K}}\right) = \begin{cases} 0.63 + 0.17\log_{10}(M/{\rm M_\odot}): & M/{\rm M_\odot} \le 0.5, \\ 0.76 + 0.59\log_{10}(M/{\rm M_\odot}): & 0.5 \le M/{\rm M_\odot} \le 1.6, \\ 1.11 + 0.30\log_{10}(M/{\rm M_\odot}): & M/{\rm M_\odot} \ge 1.6. \end{cases} \tag{A10}$$

[Note that, if we use these scalings and the relation $L_{\rm bol}/{\rm L_\odot} = (R/{\rm R_\odot})^2(T_{\rm eff}/5770\,{\rm K})^4$, instead of the $L(M)$ relation of equation (A7), we obtain ratios of $\bar{M}/\bar{L}_{\rm bol}$ for pairs of IMF models that differ by ~20 per cent, typically, from those of equation (A8)] $\bar{L}_\lambda$ values may then be computed, using the fact that $L_\lambda = \int l_\lambda(M)\psi(M)\,{\rm d}M$, where $l_\lambda(M)$, the monochromatic luminosity at wavelength λ owing to stars of mass M, is given by $l_\lambda = 4\pi R(M)^2 B_\lambda[T_{\rm eff}(M)]$, where B_λ is the Planck function, and R and $T_{\rm eff}$ come from equations (A9) and (A10).

For the two ultraviolet-based estimators of Devriendt et al. (1999) we must make conversions at $\lambda = 160$ and 280 nm, from a Salpeter (1955) IMF with mass range $[0.1,\ 120]\,{\rm M_\odot}$ to our canonical range of $[0.1,\ 100]\,{\rm M_\odot}$. The ratio of the $\bar{M}$ values for the two IMFs is unity to better than 1 per cent precision, while the $\bar{L}_\lambda$ values differ by ~10 per cent: we obtain scalings of $1.1^{1.62}$ and $1.1^{1.72}$, respectively, for the 280- and 160-nm estimators, accounting for the non-linear relationship between $\bar{L}_\lambda$ and the SFR from Devriendt et al. (1999). As before, we must account for the fact that the Cram et al. (1998) U-band estimator refers to the formation of stars of mass greater than $5\,{\rm M_\odot}$ only, when we derive its correction factor, as well as considering the difference between the $\bar{L}_\lambda$ value at 250 nm between the Cram et al. (1998) IMF and our canonical model. $\bar{M}/\bar{L}_\lambda$ for the Cram et al. (1998) IMF is only 57 per cent of that for the canonical IMF, reflecting their difference in slope, so to correct the SFR estimator of equation (2) we must multiply it by $0.57 \times 9 = 5.1$.

The 1.4-GHz estimator of Cram et al. (1998) constitutes the third class, and it is different in that it relates the SFR to the *number* of stars formed, rather than to their luminosity. As presented by Condon (1992), the argument for using decimetric radio luminosity as a measure of SFR hinges on the assumption that the radio emission from active star-forming galaxies is dominated by non-thermal emission from the remnants of Type Ib and Type II supernovae. In this picture, the radio luminosity is thus proportional to the (Type Ib and Type II) supernova rate, $\nu_{\rm SN}$, which is equated to the rate of formation of progenitors of sufficient mass ($M \ge M_0$):

$$\nu_{\rm SN} = f_{\rm N}(M \ge M_0) \times (\dot{M}/\bar{M}), \tag{A11}$$

where $f_N(M \geq M_0)$ is the fraction of stars formed that have mass $M \geq M_0$, and $\dot{M}/\bar{M}$ equals the number of stars formed per unit time. Since the decimetric radio luminosity, L_{cm}, is proportional to ν_{SN}, it follows that

$$\dot{M} \propto \left[\frac{\bar{M}}{f_N(M \geq M_0)} \times L_{cm}\right], \tag{A12}$$

which gives the correct scaling of $\dot{M}$ per unit radio luminosity between IMFs. If we follow Condon (1992) and take $M_0 = 8\,M_\odot$, we find that the $\bar{M}/f_N(M \geq M_0)$ value for our canonical IMF is 65 per cent that for the IMF assumed by Cram et al. (1998), reflecting the smaller fraction of high-mass stars in the $M^{-2.5}$ IMF, and from this we find that the factor by which the SFR given in equation (8) has to be multiplied is $0.65 \times 9 = 5.8$, where, as before, the factor of 9 corrects for the fact that equation (8) only gives the rate of formation of stellar mass in stars of mass greater than $5\,M_\odot$.

Similar procedures must be applied to convert the SFR estimates presented (for a Salpeter IMF over the mass range [1, 100] $M_\odot$) by Rigopoulou et al. (2001) to our canonical IMF: for their far-infrared estimator this is an $\bar{M}/\bar{L}_{bol}$ scaling, while for their Hα estimator we must scale by $\bar{M}/\bar{L}_\lambda$, for $\lambda = 6560$ Å. Coincidentally, we find that, in both cases, this yields a factor of 2.5 by which their SFR values must be multiplied for comparison with others computed for our canonical IMF. A further correction, however, must be applied, since Rigopoulou et al. (2001) assumed a cosmology with $\Omega_M = 0.3$ and $\Omega_\Lambda = 0.7$, which yields a larger luminosity distance out to a given redshift than does our canonical Einstein–de Sitter model. At the typical redshift ($z \sim 0.6$), this reduces the SFR estimates by ~ 30 per cent, so that the Rigopoulou et al. (2001) SFRs are to be multiplied by typical values of 1.25 before comparison with our own.

APPENDIX B: A LOGNORMAL MODEL FOR THE SAMPLING BIAS AND VARIANCE IN $\dot{\rho}_*$

We want to compute confidence ranges for $\bar{\dot{\rho}}_*$, the true, global mean SFR density at $z \sim 0.2$ and ~ 0.5 on the basis of our raw $\dot{\rho}_*$ values, given in Section 5.1. An accurate determination of these confidence ranges requires a model for the galaxy population at $0 \leq z \leq 1$ of a sophistication that is beyond the scope of this paper. However, we may obtain an estimate for them as follows.

If we denote the SFR density by X, so that the desired global mean is $\bar{X}$ and an estimate is denoted by $\hat{X}$, then we wish to determine the probability distribution $p(\bar{X}|\hat{X})$. We may adopt a Bayesian approach, writing

$$p(\bar{X}|\hat{X}) = \frac{p(\bar{X}, \hat{X})}{p(\hat{X})} = \frac{p(\hat{X}|\bar{X})p(\bar{X})}{p(\hat{X})}. \tag{B1}$$

Now, if we assume a uniform prior for $p(\bar{X})$ we find that the relative probability of $\bar{X}$ given $\hat{X}$ is

$$p(\bar{X}|\hat{X}) \propto p(\hat{X}|\bar{X}) = p(1+\delta), \tag{B2}$$

where δ is the fractional density fluctuation. Since our estimates from Section 5.2 for the variances in our two sampling volumes are of order unity, we cannot assume that the distribution of δ is Gaussian. Indeed, gravity will have skewed the distribution so that it is significantly more likely that a randomly located survey volume will be underdense than overdense, so we are more likely to have under-estimated $\bar{\dot{\rho}}_*$ than to have over-estimated it. For present purposes, we assume a lognormal model for the density field, because Bernardeau & Kofman (1995) argue that it gives a good fit to the probability density function of the density fluctuations in N-body simulations of a cold dark matter universe well into the non-linear regime (i.e. at least until the variance in fractional overdensity reaches $\sim 1.5^2$).

In the lognormal model, we have

$$p(1+\delta)\,\mathrm{d}(1+\delta) = \frac{1}{\sqrt{(2\pi\sigma_0^2)}} \times \exp\left\{-\frac{[\ln(1+\delta) + \sigma_0^2/2]^2}{2\sigma_0^2}\right\}\frac{\mathrm{d}(1+\delta)}{(1+\delta)}, \tag{B3}$$

where $\sigma_0^2 = \ln(1+\sigma^2)$ is the variance of the fictitious Gaussian field from which the true density field, with variance σ^2, is supposed to be derived, by taking the natural logarithm. It can readily be shown that $p(1+\delta)$ takes its maximum value at $1+\delta = \exp(-3\sigma_0^2/2)$, where $p(1+\delta) = \exp(\sigma_0^2)/\sqrt{(2\pi\sigma_0^2)}$.

In Fig. B1 we plot $p(1+\delta)$ against $1+\delta \equiv \hat{X}/\bar{X}$ for the three cases of $\sigma^2 = 0.5$ (dotted line), 1.0 (solid line) and 2.0 (dashed line), assuming the lognormal model of equation (B3). The relatively small fraction of area under the curves at $1+\delta > 1$ indicates the low probability that the true global mean SFR density will be lower than that estimated, reflecting the fact that for $\sigma^2 \geq 0.5$ much more of the universe is underdense than overdense. However, the mean value of $1+\delta$ must always equal unity, by definition, so our estimated SFR density is not a biased estimate, but the evolution of the cosmological density field through gravitational instability does act to increase the width of the confidence range for $\bar{\dot{\rho}}_*$ at a given percentile.

For the lognormal model, this is simple is to compute. To obtain the width of, say, the 68 per cent confidence region for $1+\delta$, we want to take the difference $z_2 - z_1$ where $z \equiv 1+\delta = z_1$ and $z = z_2$ are the solutions to the equation

$$\int_0^z p(1+\delta)\,\mathrm{d}(1+\delta) = \tilde{p} \tag{B4}$$

for $\tilde{p} = 0.16$ and 0.84 respectively. It is easy to show that

$$\int_0^z p(1+\delta)\,\mathrm{d}(1+\delta) = \frac{1}{2}\left\{1 + \mathrm{erf}\left[\frac{\ln(z) + \sigma_0^2/2}{\sqrt{2\pi\sigma_0^2}}\right]\right\}, \tag{B5}$$

where erf(x) is the error function of x, and hence to obtain 68 per

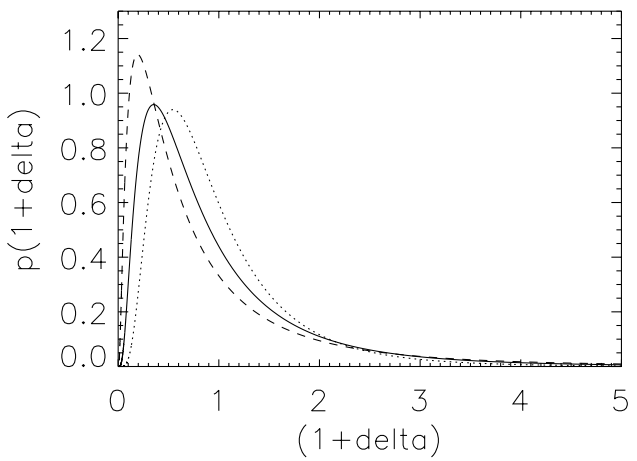

Figure B1. The probability density functions $p(1+\delta)$ as a function of $1+\delta \equiv \hat{X}/\bar{X}$ in the lognormal model for the three cases of $\sigma^2 = 0.5$, 1.0 and 2.0, plotted with dotted, solid and dashed lines respectively.

cent confidence ranges of $0.65 \leq \bar{X}/\hat{X} \leq 2.3$, $0.62 \leq \bar{X}/\hat{X} \leq 3.2$ and $0.61 \leq \bar{X}/\hat{X} \leq 5.0$, for $\sigma^2 = 0.5$, 1.0 and 2.0, respectively. It is interesting to note that, in this lognormal model, at least, the effect of continued evolution of the density field via gravitational instability is really only seen in the shift of the upper limit to the confidence interval for $\bar{X}/\hat{X}$, and that the lower limit barely changes: so, as time passes and σ^2 increases, the amount by which one's survey may have under-estimated the true, global mean SFR density increases markedly, but the amount by which it may have over-estimated it stays pretty much the same. This is equivalent to the noting that the difference between the three curves in Fig. B1 is much more pronounced at low values of $1 + \delta$, while at high values they are very close.

This paper has been typeset from a TEX/LATEX file prepared by the author.